Molecular Neurobiology (2019) 56:2073–2091
https://doi.org/10.1007/s12035-018-1208-4

Anti-prion Protein Antibody 6D11 Restores Cellular Proteostasis of Prion Protein Through Disrupting Recycling Propagation of PrP^{Sc} and Targeting PrP^{Sc} for Lysosomal Degradation

Joanna E. Pankiewicz[1,3] · Sandrine Sanchez[1] · Kent Kirshenbaum[4] · Regina B. Kascsak[5] · Richard J. Kascsak[5] · Martin J. Sadowski[1,2,3]

Received: 24 April 2018 / Accepted: 26 June 2018 / Published online: 9 July 2018

Abstract

PrP^{Sc} is an infectious and disease-specific conformer of the prion protein, which accumulation in the CNS underlies the pathology of prion diseases. PrP^{Sc} replicates by binding to the cellular conformer of the prion protein (PrP^{C}) expressed by host cells and rendering its secondary structure a likeness of itself. PrP^{C} is a plasma membrane anchored protein, which constitutively recirculates between the cell surface and the endocytic compartment. Since PrP^{Sc} engages PrP^{C} along this trafficking pathway, its replication process is often referred to as "recycling propagation." Certain monoclonal antibodies (mAbs) directed against prion protein can abrogate the presence of PrP^{Sc} from prion-infected cells. However, the precise mechanism(s) underlying their therapeutic propensities remains obscure. Using N2A murine neuroblastoma cell line stably infected with 22L mouse-adapted scrapie strain (N2A/22L), we investigated here the modus operandi of the 6D11 clone, which was raised against the PrP^{Sc} conformer and has been shown to permanently clear prion-infected cells from PrP^{Sc} presence. We determined that 6D11 mAb engages and sequesters PrP^{C} and PrP^{Sc} at the cell surface. PrP^{C}/6D11 and PrP^{Sc}/6D11 complexes are then endocytosed from the plasma membrane and are directed to lysosomes, therefore precluding recirculation of nascent PrP^{Sc} back to the cell surface. Targeting PrP^{Sc} by 6D11 mAb to the lysosomal compartment facilitates its proteolysis and eventually shifts the balance between PrP^{Sc} formation and degradation. Ongoing translation of PrP^{C} allows maintaining the steady-state level of prion protein within the cells, which was not depleted under 6D11 mAb treatment. Our findings demonstrate that through disrupting recycling propagation of PrP^{Sc} and promoting its degradation, 6D11 mAb restores cellular proteostasis of prion protein.

Keywords Endo-lysosomal system · Proteostasis · Monoclonal antibody · Passive immunization · Prion protein PrP^{Sc} conformer · Recycling propagation

Introduction

Prion diseases (prionoses) are invariably fatal, transmissible neurodegenerative diseases affecting man, primates, and several other mammalian species. Most notable examples of prionoses include Creutzfeldt-Jakob disease (CJD), Gerstmann-Straussler-Scheinker (GSS) syndrome, and kuru in man, scrapie among sheep and goats, bovine spongiform encephalopathy (BSE) in cattle, and chronic wasting disease in cervine species [1–4]. Accumulation of the disease-specific, scrapie form conformer of the prion protein (PrP^{Sc}) within the central nervous system (CNS) is a main culprit in the pathogenesis of prionoses. PrP^{Sc} is toxic, resistant to proteolysis, and replicates by binding to the cellular conformer of the prion protein (PrP^{C}) and turning its α-helix-rich conformation into its own β-sheet-dominated conformation [5, 6]. PrP^{C} is expressed on the plasma membrane, to

✉ Martin J. Sadowski
sadowm01@med.nyu.edu

1 Department of Neurology, New York University School of Medicine, 550 First Avenue, Science Building, Room 1007, New York, NY 10016, USA

2 Department of Psychiatry, New York University School of Medicine, New York, NY 10016, USA

3 Department of Biochemistry and Molecular Pharmacology, New York University School of Medicine, New York, NY 10016, USA

4 Department of Chemistry, New York University, New York, NY 10003, USA

5 New York State Institute for Basic Research in Developmental Disabilities, Staten Island, NY 10314, USA

which it is anchored by a glycophosphatidylinositol moiety arising from its carboxy terminus [7]. PrP^{C} undergoes continuous endocytic uptake and recirculation between the plasma membrane and the early endosomal compartment with turnover rate of approximately 60 min [8, 9]. The PrP^{Sc}/PrP^{C} interaction occurs on the plasma membrane and continues within the endosomal vesicles, which form a particularly enabling environment for the PrP^{C}→PrP^{Sc} conversion as their narrow internal space brings both conformers into close proximity with each another, while acidic pH facilitates transitions to β-sheet forms [10, 11]. In fact, the majority of PrP^{Sc} is generated within the endosomal compartment, which constitutes the main intracellular PrP^{Sc} reservoir [7, 12]. PrP^{Sc}-enriched endosomes are either directly recycled and trafficked back to the plasma membrane or they fuse with Golgi vesicles and interact with nascent PrP^{C} there. Degradation of PrP^{Sc} in lysosomes or by the ubiquitin-proteasome system and exocytosis of PrP^{Sc} constitute natural cellular defense mechanisms against PrP^{Sc} accumulation and cytotoxicity (reviewed in [13]). However, the relative inefficiency of these mechanisms compared to the rate of PrP^{Sc} formation allows accumulation of intracellular PrP^{Sc} as long as there is a constant supply of nascent PrP^{C} serving as a substrate for PrP^{Sc} replication. Both transfection of prion-infected cell lines with a small interfering (si) RNA targeting PrP^{C} translation [14] and conditional *Prnp* knockout in prion-infected mice [15, 16] depleted the steady-state level of PrP^{C} and subsequently resulted in disappearance of PrP^{Sc} along with attenuation of CNS pathology in infected animals. These experiments directly support the notion that natural cellular proteostatic mechanisms are capable of degrading accumulated PrP^{Sc} once its production has been curtailed.

There is currently no available treatment for prionoses. Several laboratories including our own have previously reported that selected clones of monoclonal antibodies (mAbs) raised against prion protein can permanently abrogate the presence of PrP^{Sc} from prion-infected cells [17–21]. Systemic administration of these mAbs to mice, which were inoculated with mouse-adapted scrapie strains through extra-CNS routes, significantly lowered the load of PrP^{Sc} in the lymphoid organs, effectively delaying or even preventing subsequent disease spread to the CNS [22–24]. Despite the promise demonstrated by anti-prion immunotherapy, the mechanism(s) by which therapeutic anti-prion mAbs target PrP^{Sc} replication and effect its clearance from prion-infected cells remains elusive. Our previous studies have identified a clone 6D11, which displays potent therapeutic propensity and can permanently clear PrP^{Sc} from N2A murine neuroblastoma cell line infected with 22L mouse-adapted scrapie strain (N2A/22L) at a concentration below 0.5 μg/mL [17]. The 6D11 clone was raised against PK purified 139A scrapie fibrils endowing it with high affinity to the PrP^{Sc} conformer [22, 25]. The 6D11 clone engages an epitope encompassing residues 97–100 of the murine prion protein sequence and residues 98–101 of the human prion protein sequence, which have identical amino acid order [25]. This report elucidates how this antibody interferes with the PrP^{Sc} replication and influences its clearance from N2A/22L cells.

Methods

Materials

6D11 and 4G8 mAbs were produced from their original clones using bioreactor flask and purified in house as previously described [25]. Cell culture media were obtained from Invitrogen Life Technologies (Carlsbad, CA), whereas all glass and plasticware for cell culture work were from Corning Incorporated (Corning, NY) except for 35-mm MatTek glass bottom dishes, which were from MatTek Corporation (Ashland, MA). Proteinase K (PK) and Complete Protease Inhibitor Cocktail were purchased from Roche Applied Science (Indianapolis, IN). SuperSignal Enhanced Chemiluminescent Reagent, "Restore" Western Blot Stripping Buffer, bicinchoninic acid (BCA) assay kit, and kits for cyanine 3 (Cy3) and DyLight 547 antibody labeling and Cell Surface Protein Isolation were from Pierce Biotechnology Inc. (Rockford, IL). Nitrocellulose and polyvinyl membranes and horseradish peroxidase-conjugated sheep anti-mouse secondary antibodies for immunoblotting were from GE Healthcare Life Sciences Corporation (Pittsburgh, PA), while autoradiography films X-Omat Blue XB-1 were obtained from Eastman Kodak Company (New Haven, CT). Primary antibodies against endosomal and lysosomal antigens were purchased from Santa Cruz Biotechnology (Santa Cruz, CA). Immunocytochemistry reagents mouse-on-mouse blocking solution, streptavidin/avidin blocking kit, biotinylated secondary antibodies including goat anti-mouse IgG and goat anti-rabbit IgG, and Cy3 and fluorescein isothiocyanate (FITC)-conjugated streptavidin were obtained from Vector Laboratories (Burlingame, CA). *Prnp* siRNA nucleotides and control scrambled sequence nucleotides (scRNA) were custom synthesized by Gene Link (Hawthorne, NY). All other chemicals, reagents, and antibodies were purchased from Sigma-Aldrich (St. Louis, MO).

Generation and Maintenance of Stable Prion-Infected N2A/22L Cell Line

N2A/22L line was generated by infecting N2A cells (line number CCL 131 [American Type Culture Collection; Manassas, VA]) with the 22L infectious brain homogenate, which was produced as described below [17, 22]. Immediately prior to the start of infection, 22L brain homogenate was diluted to the final concentration of 2% in Opti-MEM and 1 mL of this infectious medium was added to

sub-confluent N2A cells grown on six-well cell culture plates. After 4 h, another 1 mL of Opti-MEM supplemented with heat inactivated 10% fetal bovine serum (FBS), penicillin (100 units/mL), and streptomycin (100 μg/mL) was added to each well and the infection was carried on for another 18 h. Opti-MEM was then replaced for minimal essential medium (MEM) supplemented with 10% heat-inactivated FBS, penicillin (100 units/mL), and streptomycin (100 μg/mL) and after achieving the confluence, the cells were transferred to a 25-cm^2 flask where they were grown in the same medium until they achieved confluence again. The cells were split 1:2 every 4 to 5 days. One half of the cells was used to maintain subsequent passages of stable prion-infected line, while another half was harvested and used to monitor the level of PrP^{Sc} in each passage. This was done by PK digestion of the cell lysate followed by sodium dodecyl sulfate-polyacrylamide gel electrophoresis (SDS-PAGE) and immunoblot analysis of prion protein, as described below. All experiments were conducted on passages four through six following the infection. Control N2A cells were maintained in MEM supplemented with 10% FBS, penicillin (100 units/mL), and streptomycin (100 μg/mL) at 37 °C in 5% CO_2.

All infections of N2A cells were carried out using a single stock of 22L infectious brain homogenate. The stock was prepared as previously described [17, 22] from a pool of 10 brains harvested from CD-1 mice, when they became terminally ill as a result of intraperitoneal inoculation with 22L mouse-adapted scrapie strain. Content of PK-resistant PrP^{Sc} in the stock was verified by PK digestion and PrP^{Sc} immunoblot analysis (see below), while its infectivity was tested by inoculating CD-1 mice and confirming their transmission of prion disease. Aliquots of the 22L infectious brain homogenate were stored frozen at – 80 °C and thawed only once immediately before use. All experiments involving CD-1 mice received the approval of the NYU School of Medicine Institutional Animal Care and Use Committee.

6D11 mAb Treatment and Western Immunoblot Analysis of PrP^{Sc} and Total Prion Protein Levels

N2A/22L cells from the fifth passage following the 22L infection were plated on six-well plates and cultured in MEM supplemented with 10% heat-inactivated FBS, penicillin (100 units/mL), and streptomycin (100 μg/mL) until they reach 70–80% confluence. Then the medium was replaced with the fresh one containing 10 μg of 6D11 mAb per milliliter. The cells were harvested at various time points from the start of 6D11 mAb treatment using ice-cold lysis buffer (50 mM Tris-HCL [pH 7.5], 150 mM NaCl, 0.5% Triton X-100, 0.5% sodium deoxycholate, and Complete Protease Inhibitor Cocktail). Resulting lysates were centrifuged for 3 min at 10,000×*g* to remove cell debris and protein concentration in the resulting supernatant was determined using BCA assay. Aliquots containing 200 μg of total protein were titrated to achieve 1 μg:1 μL protein concentration and subjected to PK digestion for 30 min at 37 °C maintaining a 1:50 enzyme to protein weight ratio [17, 18]. PK activity was quenched by adding phenylmethylsulfonyl fluoride to the final concentration of 3 mM. PK-digested samples were centrifuged at 14,000×*g* for 45 min at 4 °C and the resulting supernatant was discarded. The pellets were resuspended in 30 μL sample buffer containing β-mercaptoethanol, boiled for 5 min and subjected to electrophoresis on 12.5% SDS-polyacrylamide Tris-tricine gels followed by Western transfer onto nitrocellulose membranes. PrP^{Sc} was detected using mAb 6D11 (1:3000) followed by horseradish peroxidase-conjugated sheep anti-mouse secondary antibody (1:5000) [17, 26, 27]. The membranes were developed using enhanced chemiluminescent substrate and apposed to autoradiography films over 30 s. Developed films were digitized into a 600 dpi TIFF format and analyzed using v1.47 NIH ImageJ software (Bethesda, MD). Optical densities of non-, mono-, and diglycosylated PrP^{Sc} protein bands for each sample were summed to calculate the total level of PK-resistant PrP^{Sc} [17, 22]. Values of total PrP^{Sc} level for each experimental time point obtained from three independent experiments were fitted into one-phase exponential decay equation using Graph Pad Prism v7.0c (GraphPad Software Inc. San Diego, CA).

For analysis of the total prion protein level, N2A/22L and N2A cells were lysed at different time points after the start of 6D11 mAb treatment. Cell lysate samples containing 20 μg of total protein were subjected to SDS-PAGE under reducing conditions, which immediately was followed by Western transfer into nitrocellulose membranes. The membranes were probed with 6D11 mAb and resulting autoradiography films were digitized and analyzed as described above. Equal protein loading across the samples was verified by stripping the nitrocellulose membranes and re-probing them with anti-β-actin mAb (1:1000), which protein band optical densities were analyzed using ImageJ [28].

Live Confocal Imaging of Cellular Trafficking of Cy3-Tagged 6D11 mAb

6D11 mAb was conjugated with Cy3 fluorochrome (6D11/Cy3) according to the manual provided by Pierce Biotechnology Inc. N2A/22L and N2A cells were seeded on 35-mm MatTek glass bottom dishes and maintained in Opti-MEM for 24 h before adding 2 μg of 6D11/Cy3 per milliliter of the medium. Live cells were placed in a temperature- and CO_2-controlled chamber (CTI-Controller 3700; PeCon Gmbh, Erbach, Germany) and Z stacks of confocal images were collected under a ×100 magnification and 1.4-numerical-aperture objective using Zeiss LSM 510 confocal microscope (Carl Zeiss Microscopy GmbH, Jena, Germany) at 0.5-,

1-, 4-, and 24-h time points after adding the 6D11/Cy3 mAb into the conditioned media.

To analyze intracellular accumulation of 6D11/Cy3, we determined the corrected total intracellular fluorescence (CTIF) as a modification of the widely used corrected total cellular fluorescence (CTCF) [29, 30]. This modification was required since 6D11/Cy3 avidly binds to the plasma membrane rendering the membrane strongly fluorescent. For the CTIF analysis, images representing the biggest cross-section of an analyzed cell were extracted from confocal Z stacks and the internal outline of the plasma membrane was manually traced. The integrated density as the sum of fluorescent pixel values within the traced internal cell contour was then measured. CTIF was the difference between the integrated density and the area corresponding to the selected internal cell contour multiplied by the mean fluorescence intensity of the background. Three independent experiments on both N2A and N2A/22L cell lines were carried out and 15 cells per each experimental time point and cell line were randomly selected and analyzed. All steps of the CTIF analysis were performed using NIH ImageJ v1.47.

Plasma Membrane Expression of Prion Protein

Plasma membrane-associated prion protein pool was labeled with Sulfo-NHS-SS-Biotin, which reacts with exposed primary amines of cell surface proteins but remains plasma membrane impermeable. The comparison was made across N2A and N2A/22L lines treated with 6D11 mAb (10 μg/mL) for 3, 18, and 48 h and non-treated N2A and N2A/22L cells. Immediately following the 6D11 treatment, the cells were washed twice with ice-cold PBS and incubated with Sulfo-NHS-SS-Biotin (250 μg/mL) at 4 °C for 30 min. The cells were harvested by scraping and lysing with described above lysis buffer. Nine tenth volume of each resulting cell lysate sample was passed through a NeutrAvidin Agarose Resin column, to retain Sulfo-NHS-SS-Biotin-tagged proteins, which were then eluted from the column using 50 mM dithiothreitol. Elutes were subjected to SDS-PAGE under reducing conditions and Western transfer onto nitrocellulose membranes, which were immunoblotted with 6D11 mAb as described above. Analysis of prion protein band optical densities was performed using NIH ImageJ v1.47. Remaining one tenth of sample volume was directly subjected to SDS-PAGE, Western immunoblotting, and densitometric analysis to determine total prion protein and β-actin levels within the samples as described above. Three independent surface biotinylation experiments were conducted on both N2A and N2A/22L cell lines.

Analysis of Endosomal and Lysosomal Vesicles

N2A and N2A/22L cells were plated over 24 h on round coverslips placed on the bottom of 12-well plates and treated with 6D11 mAb (10 μg/mL) for the next 4 or 24 h. Controls were cells maintained in 6D11 mAb-free medium for additional 24 h after the plating and N2A/22L cells treated with unrelated anti-Aβ mAb 4G8 (10 μg/mL) [31] for 4 or 24 h. At the conclusion of 6D11 or 4G8 mAb treatment, the cells were briefly washed three times with 37 °C PBS, fixed with 37 °C 4% paraformaldehyde for 30 min, and again thrice PBS washed to remove remaining of the fixative. Non-specific staining was blocked first with mouse-on-mouse blocking solution for 1 h followed by the streptavidin/avidin blocking kit for 30 min. Primary mAbs against early endosomal antigen (EEA1) (G-4, 1:100, mouse monoclonal), Rab7 (H-50, 1:100, rabbit polyclonal), and cathepsin D (H-75, 1:100, rabbit polyclonal) were used to immunodetect antigens specific for early endosomal, late endosomal, and lysosomal vesicles, respectively. Biotinylated goat anti-mouse IgG or goat anti-rabbit IgG secondary antibodies (both 1:1000) followed by Cy3-conjugated streptavidin (1:1000) were used to detect binding of primary antibodies to their antigens. Negative immunocytochemistry control included N2A and N2A/22L cells immunostained with omission of the primary antibodies. Z stacks of 0.2-μm-thick images of immunostained cells were captured using a Zeiss LSM 510 confocal microscope (Carl Zeiss Microscopy, Jena, Germany) and CTCF for each staining was analyzed using NIH ImageJ v1.47 [8]. Three independent experiments were carried out on both N2A and N2A/22L cell lines. Eight to 14 images containing between two and four cells per image were randomly selected for each cell line and treatment time point and analyzed.

In a parallel experiment, N2A and N2A/22L cells were plated on coverslips and treated with DyLight 547 fluorophore-tagged 6D11 mAb (6D11/DL^{547}) (10 μg/mL) for 4 or 24 h. Immediately concluding the 6D11/DL^{547} treatment, the cells were fixed, and immunostained against Rab7 or cathepsin D as described above, with the exception that FITC-conjugated secondary antibody (1:250) was used as the final step of the immunocytochemistry protocol. Z stacks of 0.2-μm-thick images of immunostained cells were captured simultaneously in FITC and rhodamine channels using a Zeiss LSM 700 confocal microscope. Captured images were then analyzed using NIH ImageJ v1.47. The amount of co-localization between 6D11/DL^{547} and Rab7 or cathepsin D in N2A and N2A/22L cells at different treatment points was quantified by computing Pearson's correlation coefficient with the help of JACoP ImageJ Plugin [32, 33]. Three independent experiments were carried out on both N2A and N2A/22L cell lines. Five to eight images containing between two and four cells per image were randomly selected for each cell line and treatment time point and analyzed.

siRNA Transfection and Analysis of PrP^{Sc} Degradation Kinetics

The *Prnp* gene was silenced using the following siRNA sequences 5′-GCC-CAG-CAA-ACC-AAA-AAC-CTT-3′ (sense)

and 5′-GGU-UUU-UGG-UUU-GCU-GGG-CTT-3′ (antisense), while the control scrambled (sc) RNA sequences were 5′-CGC-ACC-AGA-ACA-AAC-ACA-CTT-3′ (sense) and 5′-GUG-UGU-UUG-UUC-UGG-UGC-GTT-3′ (antisense) [14]. siRNA and scRNA were delivered to N2A and N2A/22L cells as a complex with DMPE-$(NaeNmpeNmpe)_3$, which is a phospholipid-oligopeptoid transfection reagent, following previously reported protocols [34]. Cells were plated on 12-well plates (10^5 cells/well) for 24 h before the transfection. For the transfection, the conditioned media were replaced with exactly 900 μL of fresh Opti-MEM medium per well. siRNA and scRNA were mixed separately with DMPE-$(NaeNmpeNmpe)_3$ in Opti-MEM at a negative:positive charge ratio of 1:3 and allowed to incubate for 10 min at room temperature. One hundred microliters of this transfection cocktail was then added to each well, followed by 100 μL of FBS 1.5 h later [34]. The final siRNA or scRNA concentrations in the conditioned media were 100 nM. At various time points after the transfection, the total level of prion protein and the PK-resistant PrP^{Sc} level were assayed in the cell lysate by Western blot densitometry as described above. In the N2A line, total prion protein levels were compared between the siRNA- and scRNA-transfected cells and control untransfected cells cultured in parallel. In the N2A/22L line, PrP^{Sc} levels were compared between siRNA- and scRNA-transfected cells, and siRNA-transfected cells co-treated with 6D11 mAb (10 μg/mL) beginning at 12 h post-transfection onward. Three independent siRNA transfection experiments were conducted on both N2A and N2A/22L cell lines.

Velocity Sedimentation in Sucrose Density Gradient

N2A cells, N2A/22L cells treated with 6D11 mAb (10 μg/mL) for 6 or 12 h, and untreated N2A/22L cells were harvested by scraping and lysing for 30 min in ice-cold HEPES buffer (20 mM HEPES [pH 7.4], 150 mM NaCl, 0.1 mM $CaCl_2$, 1 mM $MgCl_2$, and Complete Protease Inhibitor Cocktail). Insoluble cell debris were separated during 10,000×*g* centrifugation for 30 s. Two hundred microliters of supernatant collected from each sample was mixed with sarkosyl to achieve 1% of the final sarkosyl concentration and incubated for 30 min on ice [35]. Samples were then loaded on the top of 10 to 60% step sucrose gradients, which were formed by sequential layering of 300 μL of 60, 50, 40, 30, 20, and 10% sucrose concentrations in polyallomer centrifuge tubes (11 mm in diameter and 34 mm long). The gradients were centrifuged at 200,000×*g* and 4 °C for 90 min using a TLS-55 rotor in an Optima TL ultracentrifuge (Beckman Coulter, Indianapolis, IN) [36]. Spun gradients were divided into eight equal volume fractions, which were carefully collected from the top of the gradient and transferred to separate tubes. Thirty microliters from each fraction was subjected to non-reducing SDS-PAGE followed by Western transfer onto nitrocellulose membranes, which were immunoblotted with 6D11 mAb as described above. Resulting autoradiographs were densitometrically analyzed with NIH ImageJ v1.47. Optical density of prion protein bands in each fraction was converted to a percent of the sum of prion protein band optical densities in all eight fractions. In parallel, lyophilized bovine serum albumin (66.5 kDa) and apoferritin (443 kDa) were individually centrifuged in similar sucrose gradients. Following SDS-PAGE and Western transfer, these weight marker proteins were identified by Coomassie Blue stain to determine molecular weight range of prion protein oligomers trapped in each sucrose fraction. Sucrose gradient centrifugation was repeated three times, each on independently grown and 6D11 mAb-treated cells.

Detergent Solubility Assay

Untreated N2A/22L cells and N2A/22L cells treated with 6D11 mAb (10 μg/mL) for varying periods of time were harvested and lysed using ice-cold lysis buffer (50 mM Tris-HCL [pH 7.5], 150 mM NaCl, 0.5% Triton X-100, 0.5% sodium deoxycholate, and Complete Protease Inhibitor Cocktail) [37, 38] for 10 min and then warmed up to 37 °C and further incubated in the same lysis buffer at 37 °C for additional 15 min. The lysates then were centrifuged for 3 min at 10,000×*g* to remove cell debris and the total protein concentration was measured in the supernatant using the BCA assay. Aliquots containing 100 μg of total protein were titrated to a concentration of 1 μg/1 μl and then ultracentrifuged at 4 °C for 90 min at 355,000×*g* in the TLA 100.1 rotor in Optima TL ultracentrifuge [37, 38]. Resulting supernatants were transferred to new tubes while pellets containing detergent insoluble prion protein were solved in the initial volume of lysis buffer by sonication. Twenty-five-microliter samples of solubilized pellets and supernatants were mixed with 15 μL of sample buffer containing β-mercaptoethanol, boiled and subjected to SDS-PAGE separation followed by Western transfer onto nitrocellulose membranes, which were immunoblotted with 6D11 mAb as described above. Resulting autoradiographs were subjected to densitometric analysis using NIH ImageJ v 1.47. Detergent solubility assay was carried out in triplicate.

Statistical Analysis

Normal distribution within all data sets was confirmed using the Kolmogorov-Smirnov and Shapiro-Wilk tests. Differences across multiple data sets from each experiment were first interrogated using either one-way analysis of variance (ANOVA) or two-way ANOVA with 6D11 mAb treatment duration and cell line type as independent variables. Subsequent post hoc analyses exploring differences between selected pairs of data sets were carried out using Holm-Sidak's multiple comparison tests. Differences in size distribution patterns of prion protein aggregates resolved on the sucrose gradient were analyzed with two-sample Kolmogorov-Smirnov test. All statistical analyses were performed using GraphPad

Prism v 6.05 (Graph-Pad Software, Inc.). All data were reported as the mean and the standard error of the mean (SEM).

Results

6D11 mAb Establishes Exponential Decay of PrP^{Sc} Conformer with a Half-life of 10.2 h but Does Not Produce Significant Changes in the Steady-state Level of Total Prion Protein

We first investigated kinetics of PrP^{Sc} clearance from N2A/22L cells under 6D11 mAb treatment. The cells were treated with 10 μg/mL of 6D11 mAb as our previous studies showed that this concentration renders permanent PrP^{Sc} abrogation from various cell lines, which persists even after the antibody is withdrawn [17, 22]. Disappearance of the PK-resistant PrP^{Sc} signal followed exponential order kinetics. At 6, 12, and 24 h following introduction of 6D11 mAb into the conditioned media, the PrP^{Sc} signal was reduced by 28.3 ± 11.1% ($p < 0.05$), 53.7 ± 5.1% ($p < 0.001$), and 90.8 ± 3.1% ($p < 0.0001$), respectively, relative to untreated N2A/22L cells, ($p < 0.0001$, one-way ANOVA) (Fig. 1a). Forty-eight hours after the treatment was commenced, PK-resistant PrP^{Sc} was undetectable in the N2A/22L cell lysate. The half-life of PrP^{Sc} decay calculated from one-phase exponential curve was 10.2 h (Fig. 1b).

In a parallel experiment, we examined the effect of 6D11 mAb on the steady-state level of the total prion protein in N2A and N2A/22L cells by testing PK untreated samples collected at various time points during the 72-h treatment period (Fig. 1c). In the N2A line, fluctuations in the total prion protein level at any treatment time point did not exceed 8% of that in untreated cells. In N2A/22L line, the total prion protein level was reduced albeit insignificantly by 20.3 ± 11.7, 13.9 ± 10.6, and 17.5 ± 3.2% at 24-, 48-, and 72-h treatment time points, respectively (Fig. 1d). A two-way ANOVA showed no statistically significant interaction between the effect of 6D11 mAb treatment duration and cell line type on the total prion protein level ($F_{(5, 24)} = 0.39$, $p = 0.85$) and no significant main effect of either independent variable: $F_{(5, 24)} = 0.28$, $p = 0.92$ for the treatment duration, and $F_{(1, 24)} = 1.49$, $p = 0.23$ for cell line type.

6D11/Cy3 Is Internalized upon Binding at the Plasma Membrane and This Process Is More Robust in Prion-Infected Than Non-infected Cells

To interrogate how 6D11 mAb engages prion protein during its lifecycle, we tagged the antibody with Cy3 fluorophore and performed live confocal microscopy imaging of N2A and N2A/22L lines under 6D11/Cy3 treatment. Within half an hour from introducing 6D11/Cy3 mAb to the conditioned media, we observed robust fluorescent labeling of the plasma membrane in both N2A and N2A/22L lines. Modest fluorescent signals also were observed intracellularly in both cell lines at this time point. Confocal images retaken at 1, 4, and 24 h from the start of the experiment showed a progressive increase in the intracellular fluorescence, both in terms of the cross-sectional area of cells displaying the fluorescent signal and the signal intensity, which were quantified as CTIF (Fig. 2a). Comparison of CTIF values using two-way ANOVA showed statistically significant interaction between the effects of 6D11 mAb treatment duration and cell line type ($F_{(3, 98)} = 57.2$, $p < 0.0001$). At 1-, 4-, and 24-h time points, mean CTIF values in N2A cells were 3.1-, 7.8-, and 15-fold higher than that in N2A cells at 0.5-h time point, respectively, while in N2A/22L cells, they were 2.9-, 5.3-, and 20.7-fold higher than that in N2A/22L cells at 0.5-h time point, respectively ($F_{(3, 98)} = 118.8$, $p < 0.0001$ for the main effect of treatment duration). Comparison between N2A and N2A/22L cells for matching treatment time points demonstrated 3.6-, 3.5-, 2.5-, and 5-fold higher CTIF values in the latter line at 0.5, 1, 4, and 24 h, respectively ($F_{(1, 98)} = 135.9$, $p < 0.0001$ for the main effect of cell line type) (Fig. 2b). Experimental results indicate that 6D11 mAb at first engages prion protein on the plasma membrane and then undergoes internalization, which is more robust in prion-infected than in non-infected cells. These data prompted us to investigate the effect of 6D11 mAb on the plasma membrane-associated pool of prion protein and the endolysosomal system.

6D11 mAb Sequesters Prion Protein at the Plasma Membrane

To determine whether 6D11 mAb affects the pool of prion protein that is associated with the plasma membrane, we carried out cell-surface biotinylation of N2A and N2A/22L lines under 6D11 mAb treatment. In untreated cells, biotinylated prion protein constituted a relatively small fraction of the total prion protein within N2A and N2A/22L cells (Fig. 3a, c). This fraction became significantly increased under 6D11 mAb treatment in both cell lines ($p < 0.0001$ for N2A and $p = 0.0011$ for N2A/22L; one-way ANOVA). Three hours after addition of 6D11 mAb to the conditioned media, the amount of biotinylated prion protein in both N2A and N2A/22L lines increased 2.9-fold over the amount of biotinylated protein in untreated cells ($p < 0.0001$ for N2A and $p < 0.01$ for N2A/22L). The effect of 6D11 mAb on the level of biotinylated prion protein was persistent. It remained 3.2- and 3-fold higher at 18- and 48-h time points in both cell lines compared to that in untreated cells, respectively ($p < 0.0001$ for N2A at both 18 and 48 h; $p < 0.001$ and $p < 0.01$ for N2A/22L at 18 and 48 h respectively) (Fig. 3b, d).

During the cell surface biotinylation experiment, we also monitored the steady-state level of the total prion protein and β-actin (Fig. 3a, c). In 6D11 mAb-treated

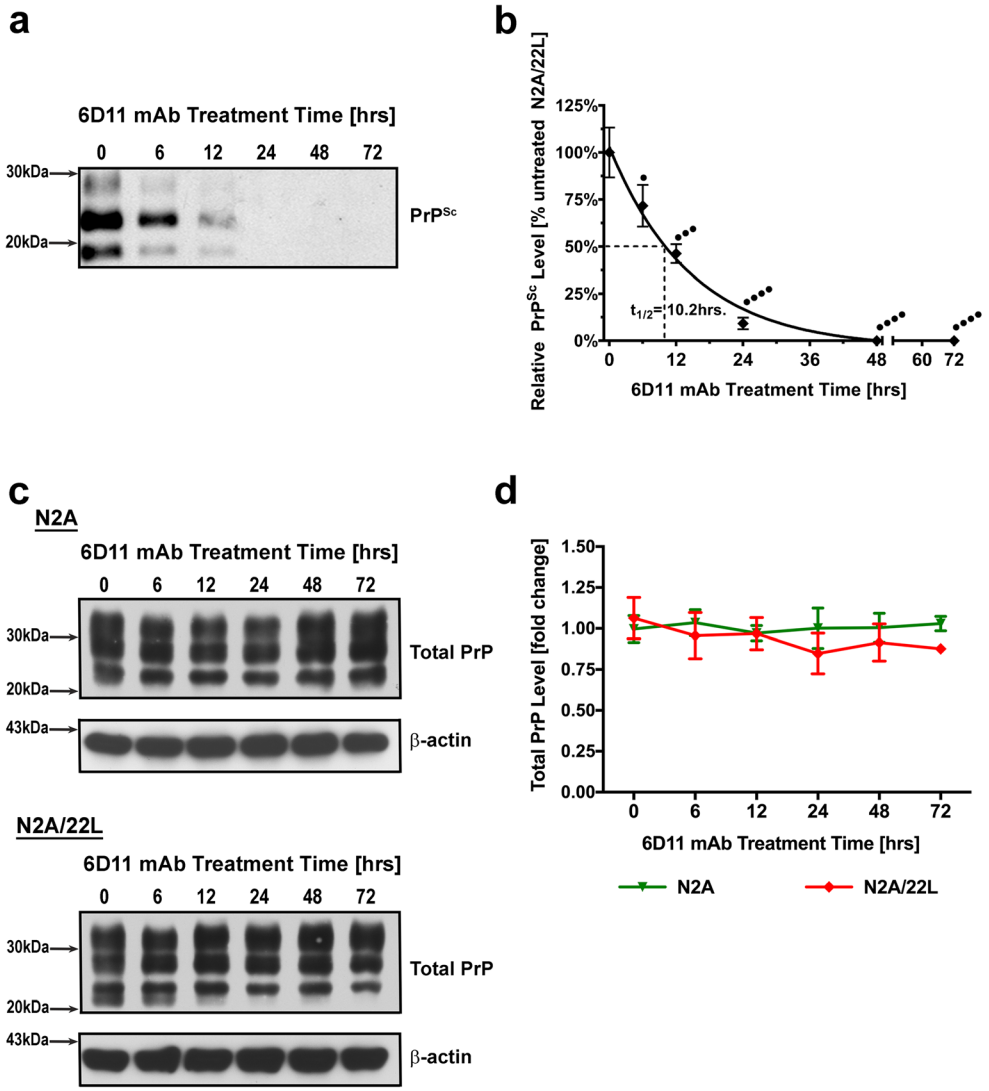

Fig. 1 Kinetics of PrP^{Sc} clearance by 6D11 mAb from N2A/22L line. 6D11 mAb treatment does not affect the steady-state level of total prion protein. **a** Immunoblot analysis of proteinase K (PK) digested PrP^{Sc} in N2A/22L cells treated with 10 μg/mL of 6D11 mAb over 72 h. **b** One phase exponential decay curve of PrP^{Sc} signal under 6D11 mAb treatment. Values represent percent of PrP^{Sc} band optical densities analyzed by densitometry relative to those in untreated N2A/22L cells averaged from three independent experiments ± standard error of the mean (SEM). PrP^{Sc} half-life ($t_{1/2}$) calculated from the slope of the curve was 10.2 h. **c** Immunoblot analyses of non-PK-digested prion protein (Total PrP) and those of β-actin in N2A and N2A/22L lines treated with 10 μg/mL of 6D11 mAb over 72 h. **d** Shown are the fold changes in the Total PrP band optical densities, which were analyzed by densitometry, normalized to β-actin, and expressed relative to those in untreated N2A and N2A/22L cells. Values represent mean and SEM from three independent experiments. **b** $p < 0.0001$ (one-way analysis of variance); $^{\bullet}p < 0.05$, $^{\bullet\bullet\bullet}p < 0.001$, and $^{\bullet\bullet\bullet\bullet}p < 0.0001$, N2A/22L cells at various treatment time points vs. untreated N2A/22L cells, respectively (Holm-Sidak's multiple comparison tests). **d** $F_{(5,\ 24)} = 0.39$, $p = 0.85$ for the interaction between 6D11 mAb treatment duration and cell line type, $F_{(5,\ 24)} = 0.28$, $p = 0.92$ for the main effect of treatment duration, and $F_{(1,\ 24)} = 1.49$, $p = 0.23$ for the main effect of cell line type (two-way analysis of variance)

cells, the total prion protein level was modestly increased (up to 1.4-fold of that in untreated cells) albeit the differences vs. untreated cells did not reach statistical significance at any time point ($p = 0.076$ for N2A line and $p = 0.077$ for N2A/22L line; one-way ANOVA). The β-actin levels showed no significant changes throughout the experiment ($p = 0.94$ for N2A line and $p = 0.23$ for N2A/22L line; one-way ANOVA) (Fig. 3b, d).

6D11 mAb Treatment Activates the Endo-lysosomal System, with Stronger Effect Observed in Prion-Infected Than in Non-infected Cells

In this experiment, we investigated whether 6D11 mAb treatment effects upregulation of the endo-lysosomal system. N2A and N2A/22L cell lines were treated with 6D11 mAb for various lengths of time, fixed, and immunostained against EEA1,

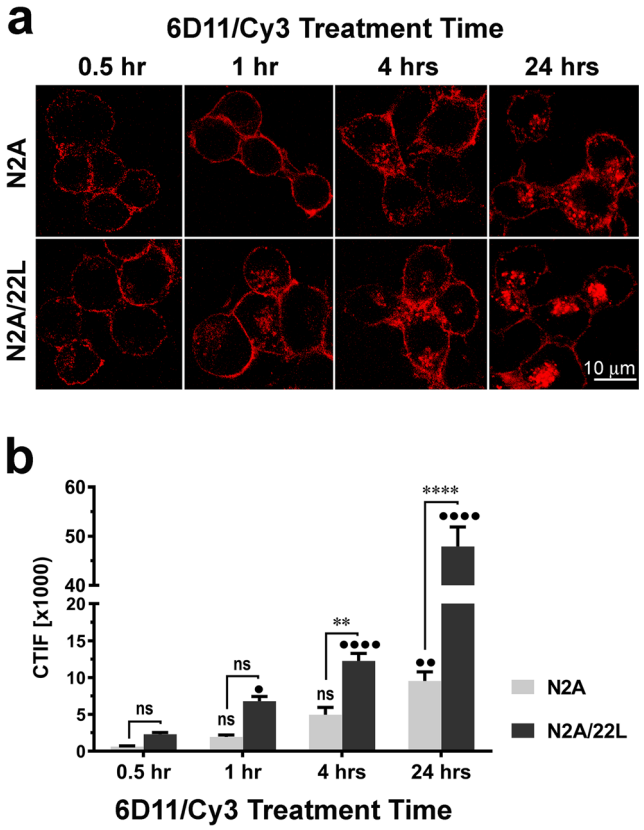

Fig. 2 Binding of 6D11/Cy3 to the plasma membrane and its ensuing internalization is significantly greater in N2A/22L than in N2A line. **a** Representative confocal microphotographs of live N2A and N2A/22L lines incubated with Cy3-conjugated 6D11 mAb (6D11/Cy3) evidencing avid binding of 6D11 mAb to the plasma membrane followed by its progressive internalization. **b** Corrected total intracellular fluorescence (CTIF) analysis revealing significantly higher internalization of 6D11/Cy3 in N2A/22L line compared to N2A line. Values are given as mean and SEM from $n = 15$ cells per line and treatment time point. **b** $F_{(3,\ 98)} = 57.23$, $p < 0.0001$ for interaction between the effects of 6D11/Cy3 mAb treatment duration and cell line type; $F_{(3,\ 98)} = 118.8$, $p < 0.0001$ for the main effect of treatment duration; and $F_{(1,\ 98)} = 135.9$, $p < 0.0001$ for the main effect of cell line type (two-way analysis of variance); $^{\bullet}p < 0.05$, $^{\bullet\bullet}p < 0.01$, $^{\bullet\bullet\bullet\bullet}p < 0.0001$; and *ns*: non-significant, N2A and N2A/22L at various treatment time points vs. N2A and N2A/22L at 0.5-h time point, respectively (Holm-Sidak's multiple comparison tests). $^{**}p < 0.01$, $^{****}p < 0.0001$, and *ns*: non-significant, N2A vs. N2A/22L for matching treatment time points (Holm-Sidak's multiple comparison tests). Scale bar 10 μm in **a**

Rab7, and cathepsin D as specific markers of early endosomal, late endosomal, and lysosomal vesicles, respectively (Fig. 4a, c, e). CTCF of immunostained cells was then analyzed and compared across the cell lines and treatment time points. There was a statistically significant interaction between the effects of cell line type and 6D11 treatment duration as revealed by two-way ANOVA on EEA1 ($F_{(2,\ 75)} = 21.2$, $p < 0.0001$) and Rab7 ($F_{(2,\ 73)} = 6.7$, $p = 0.0022$) CTCF values, but not those of cathepsin D ($F_{(2,\ 61)} = 21.2$, $p = 0.1108$) (Fig. 4b, d, f). Main effect analysis for cell line type showed EEA1, Rab7, and cathepsin D CTCF values to be significantly higher in N2A/22L line than in N2A line ($F_{(1,\ 75)} = 123.6$, $p < 0.0001$ for EEA1; $F_{(1,\ 73)} = 80.9$, $p < 0.0001$ for Rab7; and $F_{(1,\ 61)} = 52.2$, $p < 0.0001$ for cathepsin D). Main effect analysis for 6D11 mAb treatment duration also showed significant effect on CTCF values for all three endo-lysosomal markers ($F_{(2,\ 75)} = 29.6$, $p < 0.0001$ for EEA1; $F_{(2,\ 73)} = 12.8$, $p < 0.0001$ for Rab7; and $F_{(2,\ 61)} = 38.2$, $p < 0.0001$ for cathepsin D). Post hoc comparison showed EEA1, Rab7, and cathepsin D CTCF values to be 1.1-, 1.3-, and 1.4-fold higher in untreated N2A/22L cells compared to those in untreated N2A cells, respectively (significance values of post hoc analysis are shown in Fig. 4b, d, f). 6D11 mAb treatment effected progressive increase in EEA1 and Rab7 CTCF values in N2A/22L line but not in N2A line. At 4 and 24 h of 6D11 mAb treatment, EEA1 CTCF values in N2A/22L cells increased 1.6- and 1.7-fold compared to these of untreated N2A cells, respectively, while Rab7 CTCF values increased 1.5- and 1.8-fold compared to these of untreated N2A cells, respectively. In N2A line, only Rab7 CTCF value at 4 h showed a statistically significant increase compared to untreated N2A cells. Unlike EEA1 and Rab7, CTCF values for cathepsin D increased significantly following 6D11 mAb treatment in both N2A and N2A 22L lines, yet for matching treatment time points, they were significantly higher in N2A/22L line (Fig. 4f). At 4 and 24 h, cathepsin D CTCF values in N2A cells were 1.4- and 1.5-fold higher than that in untreated N2A cells, respectively, while in N2A/22L cells, they were 1.8-fold higher for both time points compared to untreated N2A cells.

In a control experiment, N2A/22L cells were treated with 4G8 mAb directed against mid-portion of the β-amyloid peptide, which is not expressed by this line, and 4G8 mAb treatment did not produce significant changes in Rab7 CTCF values ($p = 0.1634$, one-way ANOVA) (Fig. 4g, h). This negative finding indicates that increased CTCF values for various endo-lysosomal markers observed in N2A/22L line during 6D11 mAb treatment are a result of specific interaction between the 6D11 clone and prion protein expressed by this line.

6D11 mAb Is Internalized into the Endo-lysosomal Vesicles and Endo-lysosomal Compartmentalization of 6D11 mAb Is Greater in Prion-Infected Than in Non-infected Cells and Increases with Treatment Duration

Seeking a confirmation that internalized 6D11 mAb is in fact compartmentalized to the endosomal and lysosomal structures, we treated N2A and N2A/22L lines with DyLight 547 fluorophore-tagged 6D11 (6D11/DL^{547}) mAb for 4 or 24 h and then immunostained the cells against Rab7 and cathepsin D. Co-localization between 6D11/DL^{547} and anti-Rab7 or anti-cathepsin D immunostaining was assayed by determining Pearson's correlation coefficient on confocal microscopy captured images (Fig. 5a, c). A two-way ANOVA revealed no

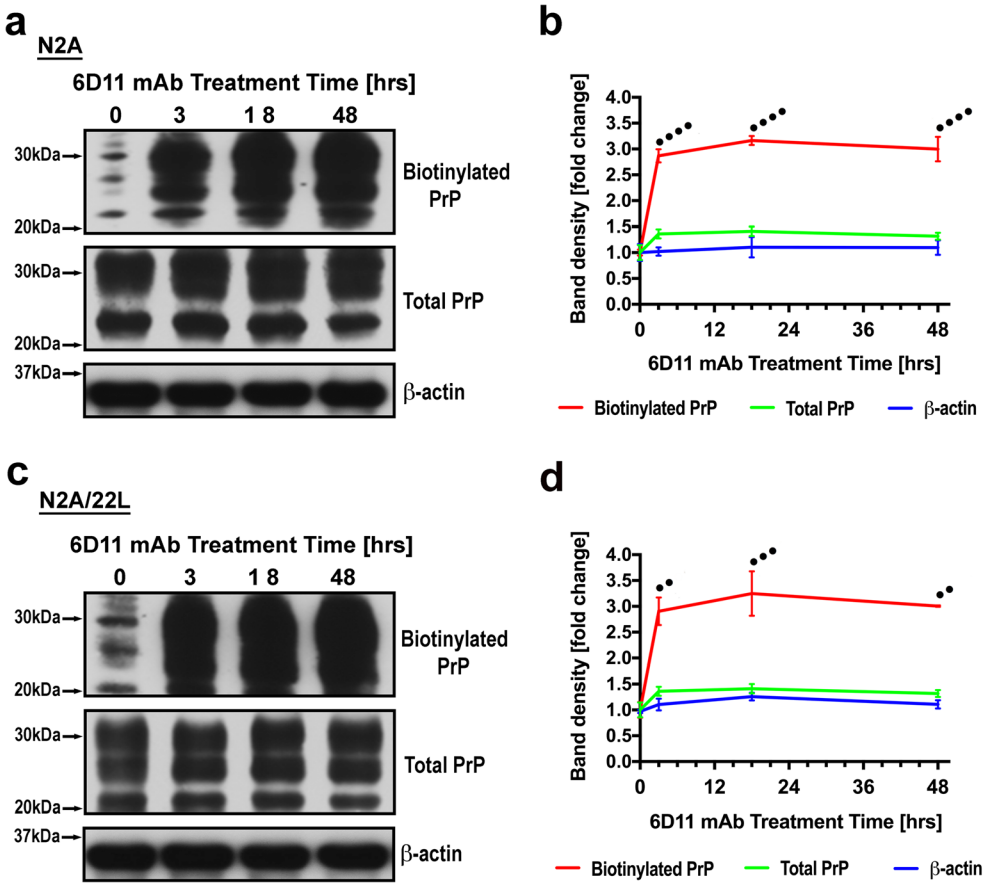

Fig. 3 6D11 mAb effects plasma membrane retention of prion protein. Immunoblot analyses of biotinylated prion protein (Biotinylated PrP), total prion protein (Total PrP), and β-actin in N2A (**a**) and N2A/22L (**c**) cells, which were treated with 10 μg/mL of 6D11 mAb for various lengths of time and subjected to surface biotinylation. Fold change of Biotinylated PrP, Total PrP, and β-actin band optical densities relative to those in untreated N2A (**b**) and N2A/22L (**d**) cells. All values represent mean and SEM from three independent experiments. **b** $p < 0.0001$ for Biotinylated PrP, $p = 0.076$ for Total PrP, and $p = 0.94$ for β-actin (one-way analysis of variance); **d** $p = 0.0011$ for Biotinylated PrP, $p = 0.077$ for Total PrP, and $p = 0.23$ for β-actin (one-way analysis of variance); $^{••}p < 0.01$, $^{•••}p < 0.001$, and $^{••••}p < 0.0001$ Biotinylated PrP level in 6D11 mAb-treated N2A and N2A/22L cells vs. its level in untreated N2A and N2A/22L cells (time = 0 h) (Holm-Sidak's multiple comparison tests). Non-significant differences are not shown on the graphs

statistically significant interaction between the effects of cell line type and treatment duration on the co-localization between 6D11/DL^{547} and Rab7 ($F_{(1,\ 24)} = 0.0002$, $p = 0.99$) and on the co-localization between 6D11/DL^{547} and cathepsin D ($F_{(1,\ 18)} = 1.92$, $p = 0.18$) (Fig. 5b, d). However, simply main effect analysis for cell line type showed that Pearson's correlation coefficient was significantly higher in N2A/22L line than in N2A line for 6D11/DL^{547} and Rab7 co-localization ($F_{(1,\ 24)} = 18.4$, $p = 0.0003$) and for 6D11/DL^{547} and cathepsin D co-localization ($F_{(1,\ 18)} = 56.9$, $p < 0.0001$). Likewise, simply main effect for treatment duration also was statistically significant both for the co-localization between 6D11/DL^{547} and Rab7 ($F_{(1,\ 24)} = 11.7$, $p = 0.0023$) and between 6D11/DL^{547} and cathepsin D ($F_{(1,\ 18)} = 5.5$, $p = 0.031$). At 4 h, Pearson's correlation coefficient between 6D11/DL^{547} and Rab7 was 0.54 ± 0.01 in N2A/22L line and increased to 0.63 ± 0.01 at 24 h while in N2A line, it was 0.42 ± 0.03 and 0.51 ± 0.04 at 4 and 24 h, respectively (significance values for pair-wise post hoc analysis are shown in Fig. 5b). For 6D11/DL^{547} and cathepsin D, Pearson's correlation coefficient was 0.55 ± 0.05 and 0.66 ± 0.02 in N2A/22L line at 4 and 24 h, respectively, while in N2A line, it was 0.37 ± 0.01 and 0.40 ± 0.04, respectively (significance values for pair-wise post hoc analysis are shown in Fig. 5d). Thus, our observations directly confirm that 6D11 mAb enters late endosomal and lysosomal vesicles and that its endo-lysosomal compartmentalization is greater in prion-infected than in non-infected cells and increases with the duration of 6D11 mAb treatment.

6D11 mAb Promotes Degradation of the PrP^{Sc} Conformer

To investigate whether 6D11 mAb directly promotes degradation of PrP^{Sc}, we compared kinetics of PrP^{Sc} decay in N2A/22L line following silencing of the *Prnp* gene with a specific siRNA in the presence and absence of 6D11 mAb. We

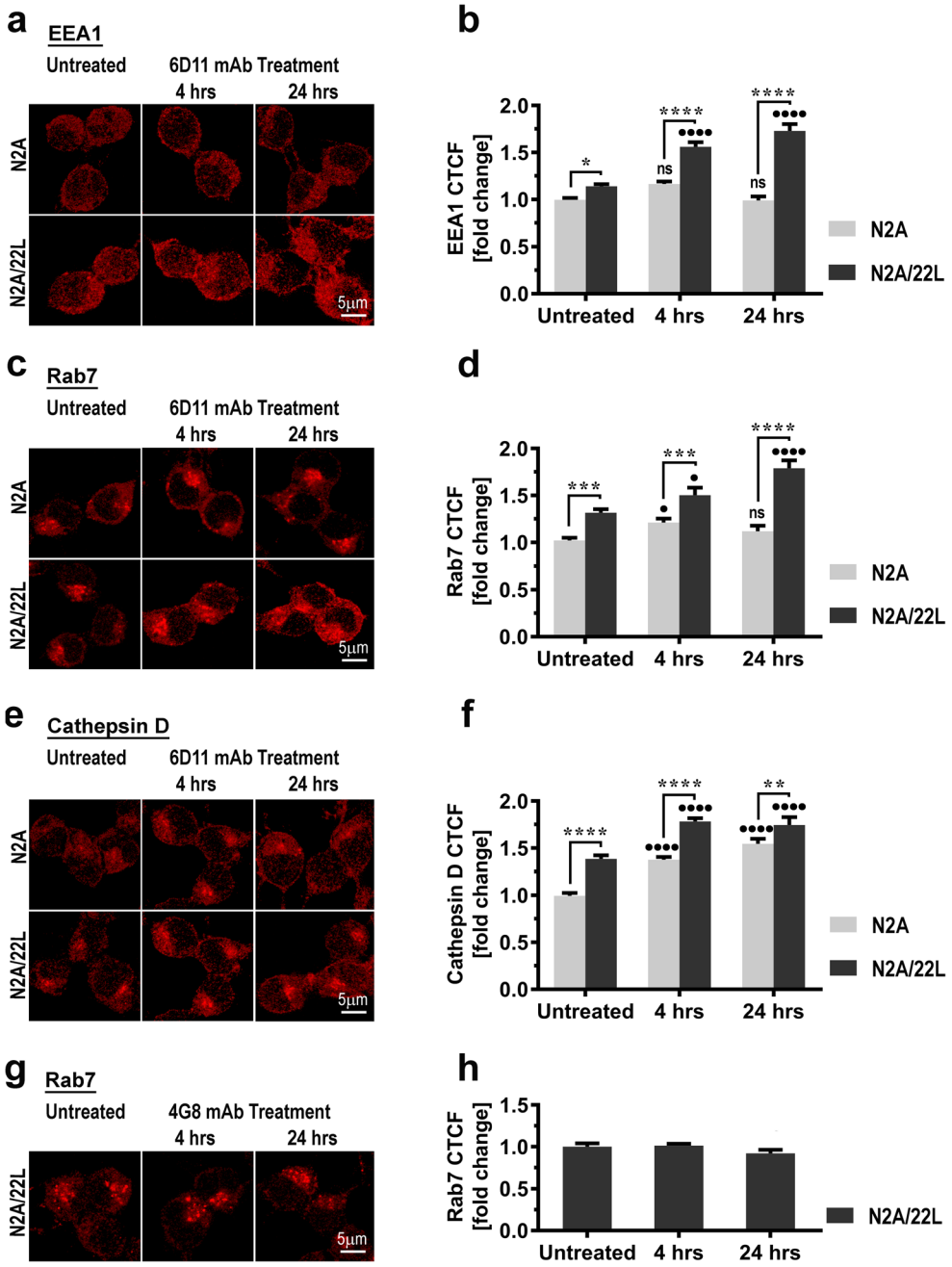

reasoned that if 6D11 mAb facilitates PrP^{Sc} degradation, we would be able to directly visualize this effect after curtailing PrP^{Sc} replication by blocking the supply of its substrate. First, we verified the specificity of the siRNA sequence to its target by comparing effects of transfection with siRNA and scRNA on the steady-state PrP^{C} level in the N2A line. A two-way ANOVA showed a statistically significant association between the effects of treatment type (siRNA vs. scRNA vs. control non-transfected cells) and treatment duration ($F_{(10,\ 36)} = 55.76$, $p < 0.0001$) (Fig. 6a, b). In addition, statistically significant associations were found for simple main effects of treatment type ($F_{(2,\ 36)} = 185$, $p < 0.0001$) and treatment duration ($F_{(5,\ 36)} = 43$, $p < 0.0001$). Sixteen hours after the siRNA transfection, the steady-state PrP^{C} level was reduced by 23.2 ± 2.0%, while at 24 and 30 h, PrP^{C} level was reduced further by 31.6 ± 2.4 and 76.5 ± 1.8% compared to non-transfected control cells, respectively (significance values for post hoc analysis are shown in Fig. 6b). No reduction in the steady-state PrP^{C} level at any analyzed time point was noted in scRNA-transfected N2A cells compared to control untransfected cells.

In a subsequent experiment, the N2A/22L line was transfected with siRNA alone, siRNA with 6D11mAb co-treatment, or with scRNA. 6D11 mAb was added into the

◀ **Fig. 4** 6D11 mAb treatment upregulates the pool of endo-lysosomal vesicles. This effect is more pronounced in N2A/22L line than in N2A line and increases with the treatment duration. Representative confocal microphotographs of N2A and N2A/22L cells treated with 6D11 mAb for various lengths of time and immunostained at the conclusion of the experiment against an early endosomal antigen EEA1 (**a**), a late endosomal marker Rab7 (**c**), and a lysosomal marker cathepsin D (**e**). **b**, **d**, **f** Corrected total cell fluorescence (CTCF) analysis of cells immunostained against EEA1, Rab7, and Cathepsin D, respectively, evidencing progressive increase in the immunostaining intensity with the treatment length and enhanced immunostaining intensity in N2A/22L line compared to N2A line for matching treatment time points. **g** N2A/22L cells immunostained against Rab7 in a control experiment where they were treated with mAb 4G8 directed against Aβ. **h** Rab 7 CTCF analysis in 4G8 mAb-treated N2A/22L cells. All values are shown as a mean and SEM from $n = 8$–14 test areas per cell line and treatment time point. **b** $F_{(2,\ 75)} = 21.2$, $p < 0.0001$ for the interaction between the effects of cell line type and 6D11 mAb treatment duration; $F_{(1,\ 75)} = 123.6$, $p < 0.0001$ for the main effect of cell line; $F_{(2,\ 75)} = 29.6$, $p < 0.0001$ for the main effect of treatment duration (two-way analysis of variance); **d** $F_{(2,\ 73)} = 6.7$, $p = 0.0022$ for the interaction between the effects of cell line type and treatment duration; $F_{(1,\ 73)} = 80.9$, $p < 0.0001$ for the main effects of cell line type; $F_{(2,\ 73)} = 12.8$, $p < 0.0001$ for the main effect of treatment duration (two-way analysis of variance); **f** $F_{(2,\ 61)} = 21.2$, $p = 0.1108$ for the interaction between the effects of cell line type and treatment duration; $F_{(1,\ 61)} = 52.2$, $p < 0.0001$ for the main effect of cell line; $F_{(2,\ 61)} = 38.2$, $p < 0.0001$ for the main effect of treatment duration (two-way analysis of variance); **b**, **d**, **f** $^{\bullet}p < 0.05$, $^{\bullet\bullet\bullet\bullet}p < 0.0001$, and *ns*: non-significant, N2A and N2A/22L cells at 4 and 24 h of 6D11 mAb treatment vs. untreated N2A and N2A/22L cells, respectively (Holm-Sidak's multiple comparison tests). $^{*}p < 0.05$, $^{**}p < 0.01$, $^{***}p < 0.001$, $^{****}p < 0.0001$, and *ns*: non-significant, N2A vs. N2A/22L for matching 6D11 mAb treatment time points (Holm-Sidak's multiple comparison tests). **g** $p = 0.1634$ (one-way analysis of variance). Scale bar 5 μm in **a**, **c**, **e**, and **g**

conditioned media at a 10 μg/mL final concentration 12 h after siRNA transfection. The lag between siRNA transfection and the start of 6D11 mAb treatment was decided based on the result of previous experiment in N2A line, where reduction in the steady-state PrP^{C} level became evident after approximately 12-h delay. Thus, the goal was to synchronize the effect of 6D11 mAb treatment (which commences nearly instantaneously after its introduction to the conditioned media, (Fig. 6a), with the onset of PrP^{C} decay effected by halting its replication. A two-way ANOVA showed a statistically significant association between the effects of treatment type (siRNA alone vs. siRNA + 6D11 vs. scRNA) and treatment duration ($F_{(10,\ 34)} = 17.3$, $p < 0.0001$) (Fig. 6c, d). Also, statistically significant were simple main effects of treatment type ($F_{(2,\ 34)} = 69.2$, $p < 0.0001$) and treatment duration ($F_{(5,\ 34)} = 43.2$, $p < 0.0001$). Eighteen hours after the start of the experiment, the steady-state PrP^{Sc} level was reduced by 58.3 ± 8.2% in N2A/22L cells transfected with siRNA alone and by 72.9 ± 6.5% in N2A/22L cells co-treated with 6D11 mAb during the siRNA transfection. At 24 and 30 h, PrP^{Sc} level was reduced by 70.7 ± 8.7 and 64.3 ± 3.1% in cells transfected with siRNA alone, respectively, and by 94.6 ± 1.1 and 93.3 ± 1.5% in the cells co-treated with 6D11 mAb during the siRNA transfection, respectively (significance values for post hoc analysis are shown in Fig. 6d). The accelerated decay of the PrP^{Sc} signal produced by 6D11 mAb in the context of inhibited PrP^{Sc} synthesis indicates that 6D11 mAb promotes PrP^{Sc} degradation. Transfection with scRNA oligonucleotides showed no statistically significant effect on the PrP^{Sc} steady-state level throughout the entire period of the experiment.

6D11 mAb Attenuates Oligomerization and Improves Solubility of Prion Protein in Prion-Infected Cells

We used velocity sedimentation in sucrose density gradient to determine whether 6D11 mAb alters the aggregation state of prion proteins in prion-infected cells. The propensity for self-assembly into oligomeric species is a well-established feature of PrP^{Sc} and of PrP^{C}/PrP^{Sc} intermediate forms, and its appearance precedes observation of PK resistance during the PrP^{C}→ PrP^{Sc} transformation process [37]. The sucrose gradient centrifugation yielded eight fractions, arbitrarily divided into upper (thin), middle, and lower (dense) fractions, which were numbered 1 through 3, 4, and 5, and 6 through 8 from the top of the sucrose gradient, respectively. Differences in the size distribution patterns of prion protein aggregates within the eight fractions were compared across untreated N2A/22L cells, 6D11 mAb-treated N2A/22L cells, and N2A cells using the two-sample Kolmogorov-Smirnov test. In untreated N2A/22L cells, prion proteins were distributed across all eight sucrose fractions. The observation of prion proteins in the lower fractions likely indicates the presence of high-order oligomeric species. 6D11 mAb treatment of N2A/22L cells effected gradual shifts in prion protein distribution from the lower and middle fractions toward the upper fractions and eventually rendered the pattern similar to that in N2A cells (Fig. 7a, b). By 6 h after the start of 6D11 mAb treatment, prion protein had already nearly disappeared from the lower fractions, while its amount increased correspondingly in the middle fractions ($p < 0.0001$, 6 h 6D11 mAb treatment vs. untreated N2A/22L cells). At 12 h of 6D11 mAb treatment, prion protein was undetectable in the lower fractions and its amount was markedly reduced in the middle fractions compared to that in untreated N2A/22L cells and those treated with 6D11 mAb for 6 h. At the same time, a compensatory increase in the amount of prion protein in the upper fractions was noticed ($p = 0.0002$, 6 vs. 12 h of 6D11 mAb treatment). The pattern of prion protein distribution across sucrose fraction in N2A/22L cells following 12 h of 6D11 treatment was similar to that of untreated N2A cells, where it was mainly detected within the upper fractions with only modest presence in the middle fractions ($p = 0.3923$, N2A/22L cells treated with 6D11 mAb for 12 h vs. N2A cells; $p < 0.0001$ N2A cells vs. untreated N2A/22L cells).

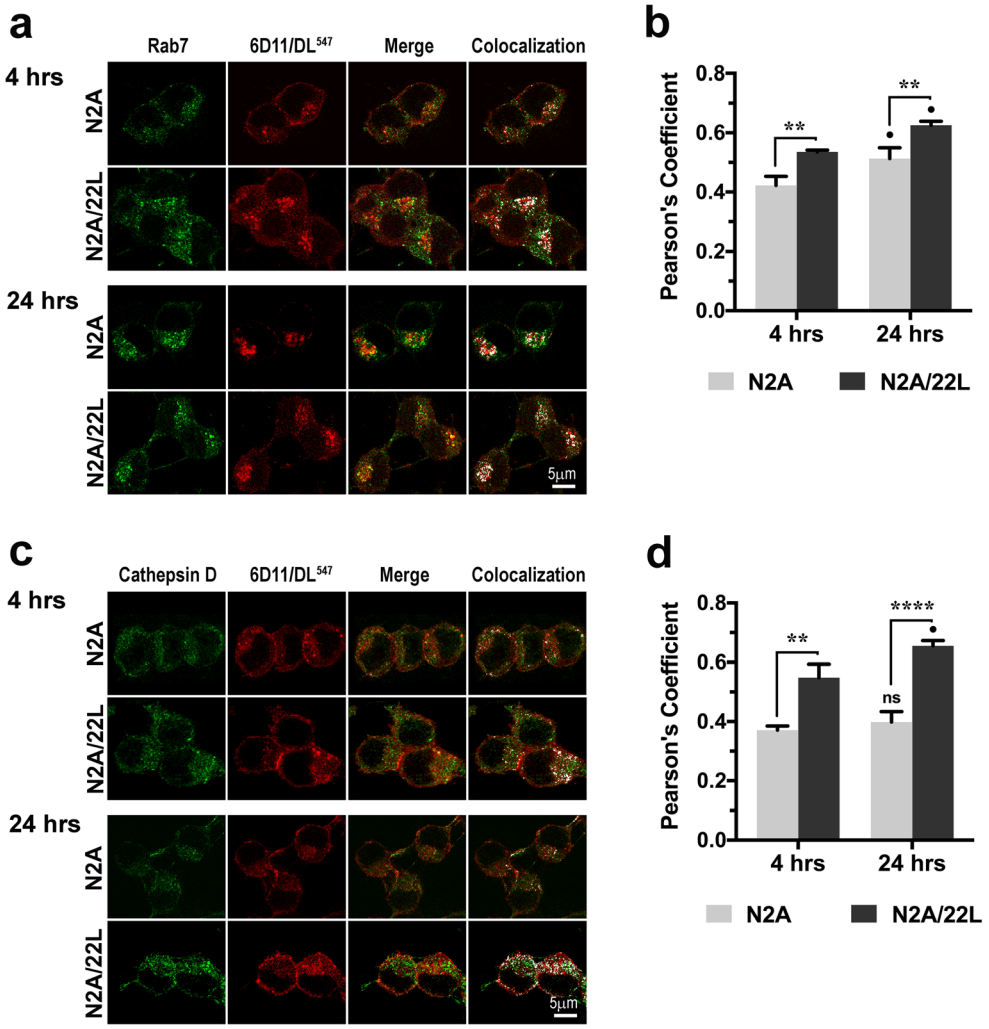

Fig. 5 Internalized 6D11/DL^{547} mAb co-localizes with late endosomal and lysosomal markers. The co-localization is greater in N2A/22L line then in N2A line and increases with the duration of 6D11/DL^{547} mAb treatment. Representative confocal microphotographs of N2A and N2A/22L cells incubated with DyLight™547 labeled 6D11 mAb (6D11/DL^{547}) mAb for 4 and 24 h and immunostained against late endosomal marker Rab7 (**a**) and lysosomal marker cathepsin D (**c**). Also shown are the digital merge of both channels and the positive co-localization (white). Pearson's correlation coefficient as a measure of co-localization between 6D11/DL^{547} mAb and anti-Rab 7 immunostaining (**b**) and between 6D11/DL^{547} mAb and anti-cathepsin D (**d**) immunostaining. Shown are means and SEM from $n = 5$–8 test areas per cell line and treatment time point. **b** $F_{(1,\ 24)} = 0.0002$, $p = 0.99$ for the interaction between the effects of cell line type and 6D11/DL^{547} mAb treatment duration; $F_{(1,\ 24)} = 18.4$, $p = 0.0003$ for the main effect of cell line type; $F_{(1,\ 24)} = 11.7$, $p = 0.0023$ for the main effect of treatment duration (two-way analysis of variance); **d** $F_{(1,\ 18)} = 1.92$, $p = 0.18$ for the interaction between the effects of cell line type and treatment duration; $F_{(1,\ 18)} = 56.9$, $p < 0.0001$ for the main effect of cell line type; $F_{(1,\ 18)} = 5.5$, $p = 0.031$ for the main effect of treatment duration (two-way analysis of variance); **b**, **d** $^{\bullet}p < 0.05$, and *ns*: non-significant, N2A and N2A/22L lines treated with 6D11/DL^{547} mAb for 24 h vs. matching lines treated for 4 h (Holm-Sidak's multiple comparison tests). $^{**}p < 0.01$, $^{****}p < 0.0001$, N2A/22L vs. N2A lines for matching treatment time points (Holm-Sidak's multiple comparison tests). Scale bar 5 μm in **a** and **c**

Reduced detergent solubility of PrP^{Sc} and PrP^{C}/PrP^{Sc} intermediates parallels their propensity to self-aggregate [37]. 6D11 mAb treatment also had a prompt effect on improving the solubility of prion protein in prion-infected cells ($p < 0.0001$, one-way ANOVA). While in untreated N2A/22L cells, the ratio of detergent soluble to detergent insoluble prion protein was 0.31 ± 0.04, within 6 h of 6D11 mAb treatment, this ratio increased 2-fold to 0.63 ± 0.05 ($p < 0.001$ vs. untreated N2A/22L cells) and after 12 and 24 h of treatment, it was further increased to 0.73 ± 0.05 and 0.78 ± 0.07 ($p < 0.0001$ vs. untreated N2A/22L cells), respectively, and remained as such until 48 h following initiation of the experiment ($p < 0.0001$) (Fig. 8a, b).

Discussion

Through a series of cell culture experiments, we sought to understand how mAb 6D11 abrogates PrP^{Sc} presence from prion-infected cells and how this effect relates to the cell

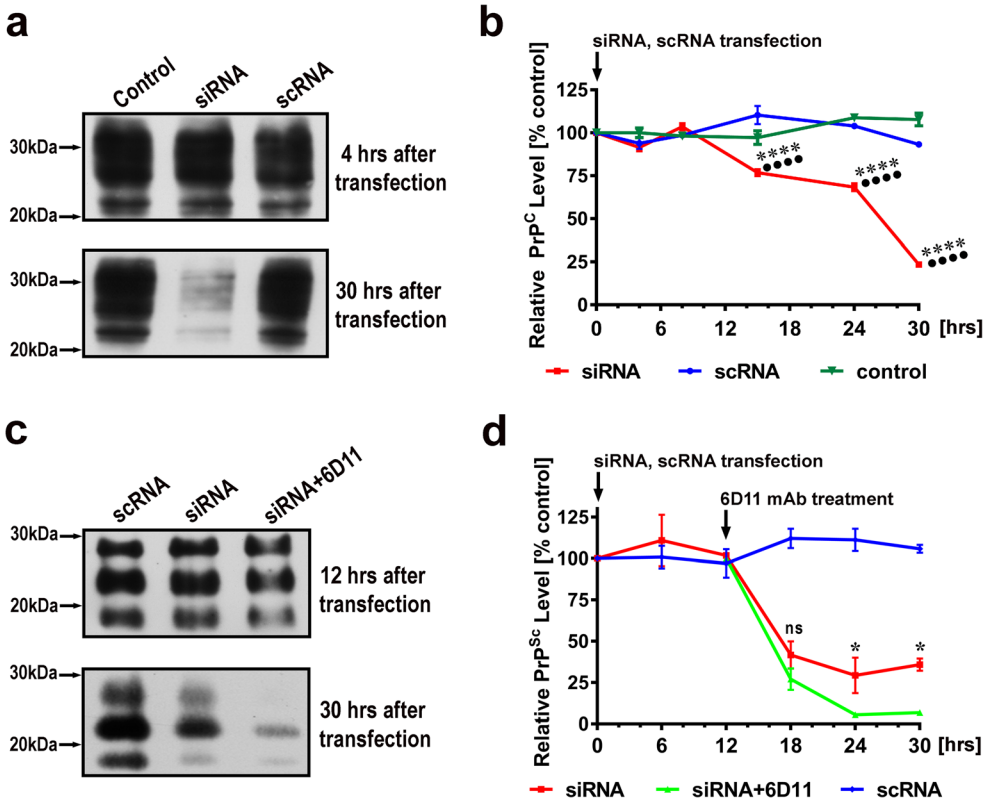

Fig. 6 Natural cellular degradation of PrP^{Sc} conformer is enhanced in the presence of mAb 6D11. Direct effect of 6D11 mAb on PrP^{Sc} degradation was determined by following the kinetics of PrP^{Sc} signal decay after blocking the formation of nascent PrP^{C} by siRNA-mediated knockdown. **a** Immunoblot analysis of the PrP^{C} steady-state level in N2A cells transfected with siRNA or scRNA and in non-transfected, control cells. **b** Analysis of PrP^{C} band optical densities reveals continuous decay of the PrP^{C} signal starting from 12 h after the siRNA but not after scRNA transfection. **c** Immunoblot analysis of PK-digested PrP^{Sc} in N2A/22L cells transfected with siRNA without and with 6D11 mAb co-treatment and in N2A/22L cells transfected with scRNA. **d** Analysis of PrP^{Sc} band optical densities demonstrates time-dependent decay of the PrP^{Sc} signal in siRNA-transfected N2A/22L cells and enhanced decay in the presence of 6D11 mAb. scRNA transfection had no effect on the steady-state PrP^{Sc} level in N2A/22L cells. Values in **b** and **d** represent mean ± SEM from three independent experiments. **b** $F_{(10,\ 36)} = 55.76$, $p < 0.0001$ for the interaction between the effects of treatment type (siRNA vs. scRNA vs. control non-transfected cells) and treatment duration; $F_{(2,\ 36)} = 185$, $p < 0.0001$ for the main effect of treatment type; and $F_{(5,\ 36)} = 43$, $p < 0.0001$ for the main effect of treatment duration (two-way analysis of variance); $^{\bullet\bullet\bullet\bullet}p < 0.0001$, siRNA-transfected N2A cells at various time points after the transfection vs. non-transfected N2A cells (Holm-Sidak's multiple comparison tests). $^{****}p < 0.0001$, siRNA-transfected N2A cells vs. scRNA-transfected N2A cells or control, cells for matching treatment time points (Holm-Sidak's multiple comparison tests). Non-significant values are not shown on the graph. **d** $F_{(10,\ 34)} = 17.3$, $p < 0.0001$ for the interaction between the effects of treatment type (siRNA vs. siRNA + 6D11 vs. scRNA) and treatment duration; $F_{(2,\ 34)} = 69.2$, $p < 0.0001$ for the main effect of treatment type; and $F_{(5,\ 34)} = 43.2$, $p < 0.0001$ for the main effect of treatment duration (two-way analysis of variance); $^{*}p < 0.05$, *ns*: non-significant siRNA vs. siRNA + 6D11 for matching treatment time points (Holm-Sidak's multiple comparison tests). Differences between siRNA or siRNA + 6D11 vs. scRNA were significant ($p < 0.0001$) at 18, 24, and 30 h (not shown on the graph). Likewise, differences between siRNA or siRNA + 6D11 at 18, 24, and 30 h but not these at 6 and 12 h vs. non-transfected N2A/22L cells (0 h) were significant ($p < 0.0001$) (not shown on the graph). At no time point, differences between scRNA and non-transfected N2A/22L cells (0 h) were significant (not shown on the graph)

trafficking cycle of prion protein. We first analyzed the kinetics of PrP^{Sc} clearance and determined that half-life of PrP^{Sc} signal decay under the 6D11 mAb treatment is 10.2 h. This tempo of PrP^{Sc} demise suggests that the modus operandi of 6D11 mAb is PrP^{Sc}-cidal rather than PrP^{Sc}-static. For comparison, PrP^{Sc}-static approaches like *Prnp* siRNA [14] or anti-PrP^{C} mAbs [18], which both target PrP^{C} steady-state level and deprive PrP^{Sc} of its replication substrate, require 4 to 6 days of constant treatment to achieve complete PrP^{Sc} demise. We also directly ruled out a possibility that 6D11 mAb depletes the steady-state PrP^{C} level, as this showed no significant changes under 6D11 mAb treatment. The fast rate of PrP^{Sc} decay in the absence of significant changes in the total prion protein level implies that 6D11 mAb may promote PrP^{Sc} degradation.

Using a fluorochrome-tagged 6D11, we also determined that 6D11 mAb engages PrP^{C} and PrP^{Sc} on the surface of the plasma membrane and the complexes formed between the antibody and the prion protein then undergo endocytic uptake. This process was significantly more pronounced in prion-infected than in non-infected cells, likely because the 6D11 clone was designed to have high affinity against the PrP^{Sc} conformer [22, 25]. Binding of 6D11 mAb to PrP^{C}

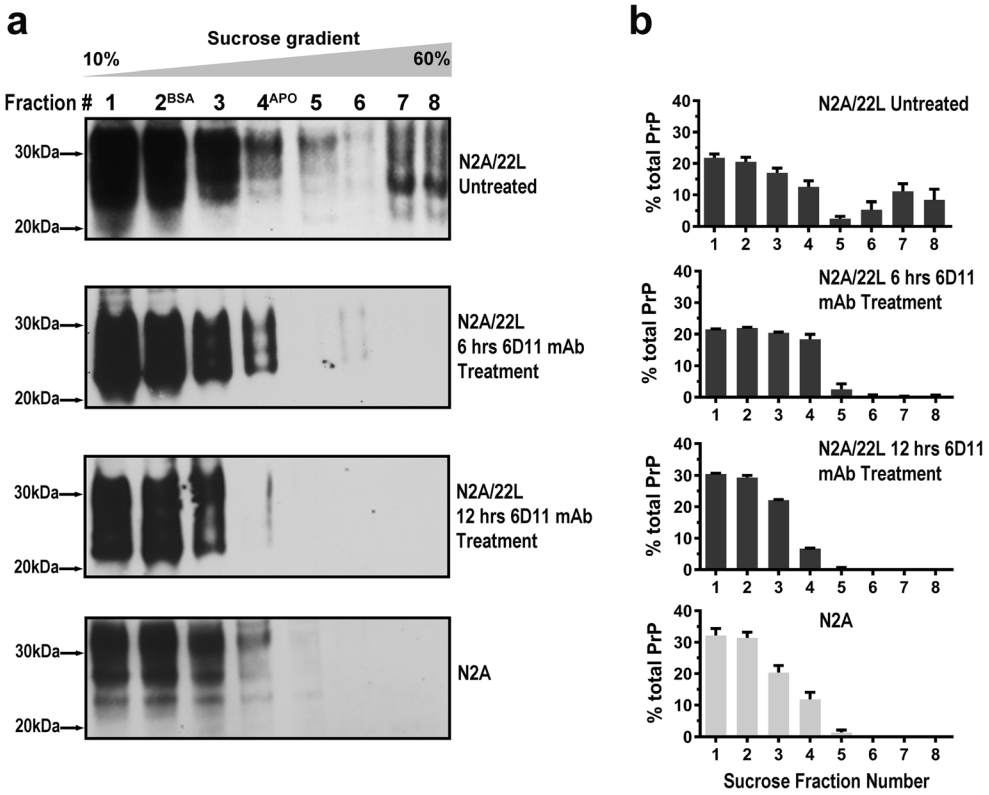

Fig. 7 mAb 6D11 treatment mitigates oligomerization of prion protein in N2A/22L cells. **a** Immunoblot analyses of prion protein in lysates from untreated N2A/22L cells, N2A/22L cells treated with mAb 6D11 for 6 or 12 h, and these from N2A cells subjected to velocity sedimentation in a step sucrose gradient. Bovine serum albumin (BSA) (68 kDa) and apoferritin (APO) (443 kDa) were used as molecular weight markers and under the same sedimentation conditions, they were found emerged in fractions 2 and 4, respectively. **b** Size distribution graphs of prion protein across eight sucrose fractions in untreated N2A/22L cells, 6D11 mAb-treated N2A/22L cells, and these from N2A cells, which examples are shown in **a**. Values represent percent of prion protein band optical density analyzed by densitometry in a given fraction relative to the sum of all band optical densities in eight fractions. Shown are the mean and SEM from three independent experiments. There was a significant shift in the prion protein distribution pattern in N2A/22L cells effected by 6D11 mAb treatment. Reduction in prion protein distribution in the lower (6–8) and middle (4–5) fractions occurred over time with compensatory increase in the upper fractions (1–3) eventually rendering the pattern in 12-h 6D11 mAb-treated N2A/22L cells similar to that in N2A cells. Differences in prion protein size distribution patterns across the eight sucrose fractions were analyzed using two-sample Kolmogorov-Smirnov test and were found to be significantly different between untreated N2A/22L cells and N2A cells ($p < 0.0001$); untreated N2A/22L cells and N2A/22L cells treated with 6D11 mAb for 6 h ($p < 0.0001$); N2A/22L cells treated with 6D11 mAb for 6 h; and these treated for 12 h ($p = 0.0002$); but not between N2A/22L cells treated with 6D11 mAb for 12 h and N2A cells ($p = 0.3923$)

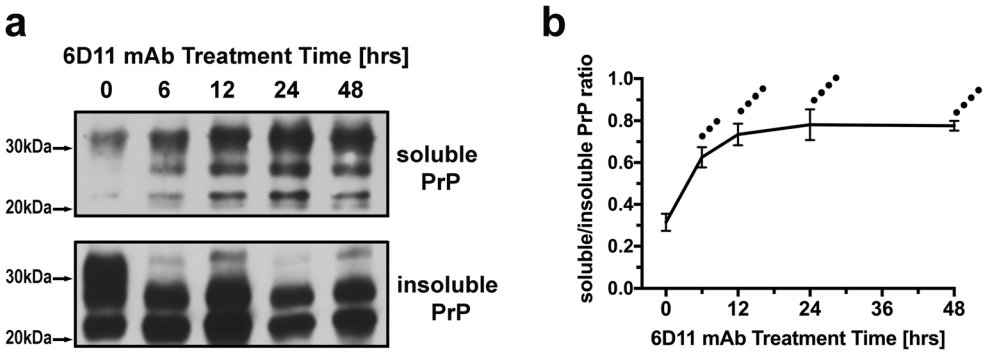

Fig. 8 mAb 6D11 increases solubility of prion protein in N2A/22L cells. **a** Immunoblot analysis of detergent soluble and detergent insoluble prion protein fractions in N2A/22L cells treated with 6D11 mAb for various lengths of time. **b** Ratio of soluble to insoluble prion protein band optical densities shown as mean values ± SEM from three independent experiments as in **a**. **b** $p < 0.0001$ (one-way analysis of variance); $^{\bullet\bullet\bullet}p < 0.001$, $^{\bullet\bullet\bullet\bullet}p < 0.0001$ vs. untreated N2A/22L cells (time = 0 h) (Holm-Sidak's multiple comparison tests)

and PrP^{Sc} on the cell surface resulted in a 3-fold increase in the amount of plasma membrane-associated prion protein without significant changes in its total steady-state level within the cell. The retention of prion protein on the plasma membrane likely disturbs its constitutive cycling between the cell surface and the endocytic compartment, which underlies the mechanism of PrP^{Sc} propagation. We also found that subsequent endocytosis of PrP^{C}/6D11 and PrP^{Sc}/6D11 complexes from the plasma membrane influenced activation of the endo-lysosomal system. Significant increases in CTCF values for early endosomal marker EEA1, late endosomal marker Rab7, and lysosomal marker cathepsin D were found in 6D11 mAb-treated prion-infected cells. Likewise, in non-infected cells, 6D11 mAb treatment effected significant increase in CTCF values for cathepsin D, while it had a less consistent effect on upregulation of EEA1 and Rab7 CTCFs. Through a co-localization analysis, we directly demonstrated that upon internalization, 6D11 mAb is compartmentalized to the late endosomes and lysosomes and that its presence there progressively increases with the treatment and is significantly higher in prion-infected than in non-infected cells. This evidence collectively indicates that following endocytosis, the complexes between antibody and prion protein pass through the early and late endosomes and proceed to the lysosomes, where likely undergo degradation. Of note, under physiological conditions with each trans-cellular trafficking cycle, 95% of prion protein endocytosed from the plasma membrane departs from the endo-lysosomal pathway at the level of early endosomes and returns to the plasma membrane through recycling endosomes, while only 5% undergoes intracellular proteolysis [8, 9]. The activation of the endo-lysosomal system was specifically related to formation of the complexes between prion protein and 6D11 mAb and their endocytosis as in a control experiment where N2A/22L cells were treated with a mAb directed against human Aβ sequence, which is not expressed by these cells, no effect on Rab7 CTCF values was seen. We also observed modest upregulation of endo-lysosomal markers in untreated N2A/22L cells when comparing them to untreated N2A cells, which likely reflects the inherent involvement of the endo-lysosomal system in prion pathology, a feature more prominently observed in non-dividing cells such as neurons in CJD brains [39, 40]. Increased targeting of prion protein to lysosomes by the 6D11 mAb was associated with its increased degradation. This was directly demonstrated in prion-infected cells in which formation of nascent PrP^{Sc} was abolished by siRNA silencing of PrP^{C} translation. Co-treatment of these cells with 6D11 mAb resulted in significant acceleration of the PrP^{Sc} signal decay. Figure 9 illustrates the

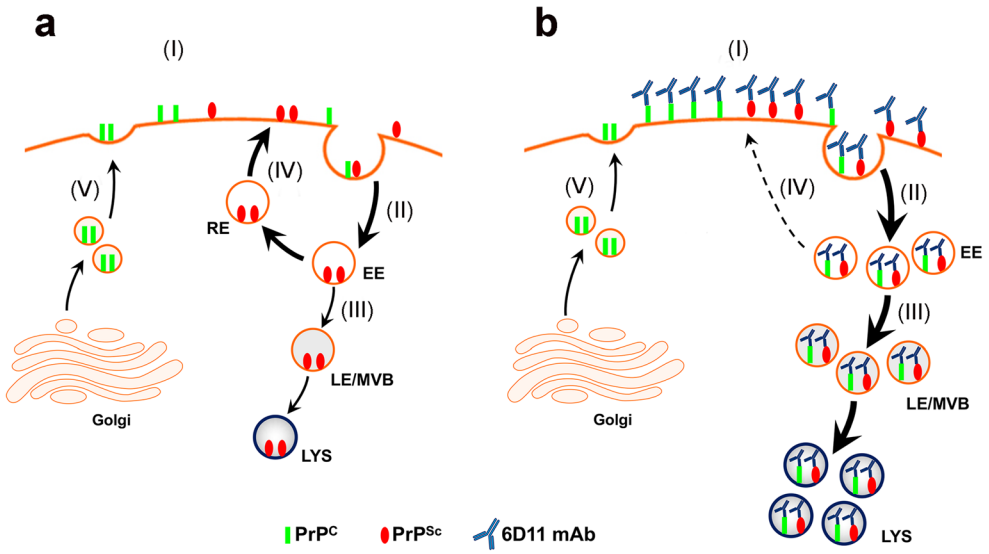

Fig. 9 Therapeutic effect of 6D11 clone depends on disrupting cellular trafficking of prion protein and promoting lysosomal degradation of PrP^{Sc}. **a** A diagram of PrP^{C} and PrP^{Sc} conformers trafficking between the cell surface and endocytic compartment in prion-infected cells. (I) Plasma membrane-attached PrP^{C} and PrP^{Sc} undergo continuous endocytosis. (II) Close contact between both conformers in the endosomes facilitates PrP^{C}→ PrP^{Sc} transformation. (III) Relatively minor portion of PrP^{Sc} containing early endosomes is directed toward late endosomes and subsequently to lysosomes for degradation, (IV) while relatively larger pool of early endosomes recycles back to the plasma membrane delivering nascent PrP^{Sc}. (V) Natively translated and Golgi maturated PrP^{C} is transported to the plasma membrane and serves as a substrate for continuous PrP^{Sc} replication. **b** Proposed modus operandi of therapeutic 6D11 clone: (I) 6D11 mAb binds PrP^{C} and PrP^{Sc} on the plasma membrane effecting their sequestration there. (II) 6D11/PrP^{C} and 6D11/PrP^{Sc} complexes undergo enhanced endocytosis, while 6D11 mAb precludes PrP^{C}/PrP^{Sc} interaction in the endosomal compartment hampering PrP^{C}→PrP^{Sc} conversion. (III) 6D11/PrP^{C} and 6D11/PrP^{Sc} complexes are preferentially directed for lysosomal degradation, (IV) while the amount of PrP^{Sc} returning to the plasma membrane is greatly reduced. (V) Newly translated PrP^{C} reconstitutes overall pool of prion protein depleted by enhanced lysosomal degradation effected by 6D11 mAb. EE early endosomes, MVB multivesicular bodies, LE late endosomes, LYS lysosomes, RE recycling endosomes

proposed modus operandi of 6D11 mAb for clearance of PrP^{Sc} from prion-infected cells. We posit that 6D11 mAb sequesters a pool of PrP^{C} and PrP^{Sc} on the plasma membrane slowing down the tempo of their constitutive cycling between the cell surface and the endocytic compartment (Fig. 9a). PrP^{C}/6D11 and PrP^{Sc}/6D11 complexes are then subsequently cleared from the plasma membrane through active endocytosis, but unlike antibody-free prion protein, which promptly recycles back to the plasma membrane, these complexes are largely directed to late endosomes and then on to lysosomes for degradation (Fig. 9b). Ongoing translation of prion protein provides constant source of nascent PrP^{C}, which precludes depletion of its steady-state level in the cell. Thus, anti-PrP mAbs, such as the 6D11 clone, provide an interesting approach to restore disturbed proteostasis of prion protein in prion-infected cells. Likewise, several other strategies focused on stimulating PrP^{Sc} degradation also have demonstrated efficacy in experimental models of prionoses [13].

The 6D11 clone was raised against PK purified 139A scrapie fibrils endowing its high affinity to the PrP^{Sc} conformer [22, 25]. Only a small number of all clones raised against prion protein that including 6D11 have been shown to completely abrogate the presence of PrP^{Sc} from infected cells and all of these therapeutic clones are able to recognize the PrP^{Sc} conformer [17–19, 21, 23–25, 41]. The proposed modus operandi of the 6D11 mAb may rationalize this prerequisite, as the clones with therapeutic properties need to effectively engage native PrP^{Sc} exposed on the surface of the plasma membrane. Another feature frequently found among the clones with therapeutic properties is the location of their epitopes within the central fragment of the prion protein. Most of these clones have the epitope located along residues 90 through 105 or along residues 130 through 156 of the prion protein sequence, with 6D11 clone belonging to the first group [17–19, 21, 23–25, 41]. There are several lines of evidence to indicate that the sequence along residues 90–156 plays an essential role in engaging the physical contact between PrP^{Sc} and PrP^{C}, and undergoes significant conformational refolding during $PrP^{C}\rightarrow PrP^{Sc}$ transformation [42, 43]. Through direct binding the central region of the PrP^{Sc} conformer, these therapeutic clones likely promote steric hindrance of the domain responsible for the direct PrP^{Sc}/PrP^{C} interaction, and this effect may play a particularly important role within the narrow internal space of endosomal vesicles which brings both PrP^{Sc} and PrP^{C} conformers into close proximity with each another [10].

PrP^{Sc} is transformed from the nascent PrP^{C} during a relatively protracted process, with an estimated half-life of ~ 15 h [7]. Prior to attainment of PK resistance, PrP^{C}/PrP^{Sc} intermediates already display altered physico-chemical properties including reduced detergent solubility and enhanced propensity for self-aggregation [10, 37, 38]. These also are invariable features of the PrP^{Sc} conformer itself. We determined that 6D11 clone attenuated oligomerization prion protein in prion-infected cells. A significant anti-oligomerization effect was seen within 6 h of the treatment, while after 12 h, distribution of prion protein across sucrose fractions was comparable to that in non-infected cells. Since attenuation of prion protein aggregability significantly precedes the total abrogation of PrP^{Sc}, it is likely that 6D11 mAb targets PrP^{C}/PrP^{Sc} intermediate forms possibly through hindrance and stabilization of the central region of the prion protein. Similarly, detergent solubility of prion protein showed significant improvement under the 6D11 mAb treatment; however, its timing was more closely associated with that of disappearance of the PrP^{Sc} signal and likely reflects such.

Immunization strategies against disease-specific misfolded proteins are being actively pursued as therapeutic approaches for Alzheimer's disease [44, 45], non-Alzheimer's tauopathies [46], and α-synucleinopathies [47]. Though in comparison to these entities, prionoses are relatively infrequent, they are nevertheless invariably fatal within a year to a few years from the time of diagnosis. Certain forms of prionoses are known to be effectively transmitted to humans through extra-CNS inoculation routes and constitute a tangible clinical problem. Perhaps the most notable example is a variant CJD (vCJD) caused by ingestion of meat products from BSE-infected cattle [48]. Though the incidence of vCJD has been sharply decreasing after 2011, new cases are still emerging due to prolonged pre-CNS replication period of PrP^{Sc} within the lymphoid tissue [49–52] and individual genetic susceptibility to prion diseases [53, 54]. This lingering vCJD incidence also is associated with a phenomenon of silent vCJD carriers. These are neurologically asymptomatic individuals harboring PrP^{Sc} within extra-CNS tissues who constitute a dangerous source of sequential transmission of prionoses among humans [55]. To date, there have been four tallied cases of CJD spread through transfusion of blood products derived from vCJD patients who were asymptomatic during the time of blood donation [56]. One study aiming to estimate the prevalence of asymptomatic carriers resulting from the BSE epidemics in the UK suggested their prevalence to be as high as 1:4000 making a possibility of secondary CJD spread from these individuals a tangible public health concern [57]. On the other hand, the extended period of peripheral PrP^{Sc} replication that precedes neuroinvasion creates a promising window of opportunity for employing preventive therapies, such as passive immunization. In fact, we and others have shown that targeting PrP^{Sc} replication within the lymphoid tissue using therapeutic clones like 6D11 lowers peripheral PrP^{Sc} load, significantly delays neuroinvasion, and increases the lifespan of peripherally inoculated mice [22–24]. In contrast to successful targeting of peripheral PrP^{Sc} replication, passive immunization studies in animal models of prionoses showed limited effects against replication of PrP^{Sc} within the CNS [23]. This limitation is an effect of poor blood-brain barrier penetrance of antibodies, making the prospect of developing

immunization-based therapies for symptomatic subjects more challenging. To meet this challenge, several approaches including intrathecal delivery of antibodies via osmotic pump [58], use of smaller, single-chain variable fragment antibodies [59, 60], and intrathecal antibody expression using a viral vector [61, 62] have been proposed and tested in animal models of prionoses. These approaches showed both promising efficacy and safety [63].

Conclusion

Our study examined the modus operandi of the 6D11 mAb clone for abrogating PrP^{Sc} presence from prion-infected cells. Its action features disruption of the recycling and propagation of PrP^{Sc} between the cell surface and the endocytic compartment where PrP^{Sc} recruits PrP^{C}, instead directing PrP^{Sc} to lysosomes for degradation. By shifting the balance between PrP^{Sc} formation and degradation, the 6D11 clone restores cellular proteostasis of the prion protein. Studies providing mechanistic insight into the therapeutic effect of mAbs also can inform the design of other, small molecular therapeutic agents for treatment of prion diseases.

Funding This work was supported by the following awards from the National Institute on Aging R01 AG029635 (MJS), R01 AG031221 (MJS), and R01 AG053990 (MJS), and by the following award from the National Science Foundation CHE-1507946 (KK).

Compliance with Ethical Standards

All mouse care and experimental procedures were approved by the Institutional Animal Care and Use Committee of the New York University School of Medicine.

Conflict of Interest JEP, SS, KK, and MJS declare no competing interests. RBK and RJK receive royalties for licensing the 6D11 clones, which currently is marketed by BioLegend (San Diego, CA).

References

1. Sadowski M, Kumar A, Wisniewski T (2008) Prion diseases. In: Bradley WG (ed) Neurology in clinical practice,. 5th edition edn. Butterworth-Heinemann, pp. 1567–1581
2. Mackenzie G, Will R (2017) Creutzfeldt-Jakob disease: recent developments. F1000Research 6:2053. https://doi.org/10.12688/f1000research.12681.1
3. Geschwind MD (2015) Prion diseases. Continuum (MinneapMinn):1612-1638. doi:https://doi.org/10.1212/CON.0000000000000251 00132979-201512000-00011
4. Aguilar-Calvo P, Garcia C, Espinosa JC, Andreoletti O, Torres JM (2015) Prion and prion-like diseases in animals. Virus Res 207:82–93. https://doi.org/10.1016/j.virusres.2014.11.026
5. Aguzzi A, Lakkaraju AK (2016) Cell biology of prions and prionoids: a status report. Trends Cell Biol 26(1):40–51. https://doi.org/10.1016/j.tcb.2015.08.007
6. Prusiner SB (2001) Neurodegenerative diseases and prions. N Engl J Med 344(20):1516–1526
7. Borchelt DR, Scott M, Taraboulos A, Stahl N, Prusiner SB (1990) Scrapie and cellular prion proteins differ in their kinetics of synthesis and topology in cultured cells. J Cell Biol 110(3):743–752
8. Harris DA (1999) Cell biological studies of the prion protein. Curr Issues Mol Biol 1(1–2):65–75
9. Shyng SL, Huber MT, Harris DA (1993) A prion protein cycles between the cell surface and endocytic compartment in cultured neuroblastoma cells. J Biol Chem 268:15922–15928
10. Harris DA (1999) Cellular biology of prion diseases. Clin Microbiol Rev 12(3):429–444
11. Borchelt DR, Taraboulos A, Prusiner SB (1992) Evidence for synthesis of scrapie prion proteins in the endocytic pathway. J Biol Chem 267(23):16188–16199
12. Jeffrey M, McGovern G, Siso S, Gonzalez L (2011) Cellular and sub-cellular pathology of animal prion diseases: relationship between morphological changes, accumulation of abnormal prion protein and clinical disease. Acta Neuropathol 121(1):113–134. https://doi.org/10.1007/s00401-010-0700-3
13. Goold R, McKinnon C, Tabrizi SJ (2015) Prion degradation pathways: potential for therapeutic intervention. Mol Cell Neurosci 66, 12:–20. https://doi.org/10.1016/j.mcn.2014.12.009
14. Daude N, Marella M, Chabry J (2003) Specific inhibition of pathological prion protein accumulation by small interfering RNAs. J Cell Sci 116:2775–2779
15. Mallucci G, Dickinson A, Linehan J, Klohn PC, Brandner S, Collinge J (2003) Depleting neuronal PrP in prion infection prevents disease and reverses spongiosis. Science 302(5646):871–874. https://doi.org/10.1126/science.1090187
16. Mallucci GR, White MD, Farmer M, Dickinson A, Khatun H, Powell AD, Brandner S, Jefferys JG et al (2007) Targeting cellular prion protein reverses early cognitive deficits and neurophysiological dysfunction in prion-infected mice. Neuron 53(3):325–335. https://doi.org/10.1016/j.neuron.2007.01.005
17. Pankiewicz J, Prelli F, Sy MS, Kascsak RJ, Kascsak RB, Spinner DS, Carp RI, Meeker HC et al (2006) Clearance and prevention of prion infection in cell culture by anti-PrP antibodies. Eur J Neurosci 23(10):2635–2647
18. Perrier V, Solassol J, Crozet C, Frobert Y, Mourton-Gilles C, Grassi J, Lehmann S (2004) Anti-PrP antibodies block PrPSc replication in prion-infected cell cultures by accelerating PrP degradation. J Neurochem 89(2):454–463
19. Enari M, Flechsig E, Weissmann C (2001) Scrapie prion protein accumulation by scrapie-infected neuroblastoma cells abrogated by exposure to a prion protein antibody. Proc Natl Acad Sci U S A 98(16):9295–9299
20. Xiao Q, Yan P, Ma X, Liu H, Perez R, Zhu A, Gonzales E, Burchett JM et al (2014) Enhancing astrocytic lysosome biogenesis facilitates Abeta clearance and attenuates amyloid plaque pathogenesis. J Neurosci 34(29):9607–9620. https://doi.org/10.1523/JNEUROSCI.3788-13.2014
21. Peretz D, Williamson RA, Kaneko K, Vergara J, Leclerc E, Schmitt-Ulms G, Mehlhorn IR, Legname G et al (2001) Antibodies inhibit prion propagation and clear cell cultures of prion infectivity. Nature 412(6848):739–743
22. Sadowski MJ, Pankiewicz J, Prelli F, Scholtzova H, Spinner DS, Kascsak RB, Kascsak RJ, Wisniewski T (2009) Anti-PrP Mab 6D11 suppresses PrP^{Sc} replication in prion infected myeloid precursor line FDC-P1/22L and in the lymphoreticular system in vivo. Neurobiol Dis 34(2):267–278
23. White AR, Enever P, Tayebl M, Mushens R, Linehan J, Brandner S, Anstee D, Collinge J et al (2003) Monoclonal antibodies inhibit prion replication and delay the development of prion disease. Nature 422:80–83

24. Heppner FL, Musahl C, Arrighi I, Klein MA, Rulicke T, Oesch B, Zinkernagel RM, Kalinke U et al (2001) Prevention of scrapie pathogenesis by transgenic expression of anti-prion protein antibodies. Science 294(5540):178–182
25. Spinner DR, Kascsak RB, LaFauci G, Meeker HC, Ye X, Flory MJ, Kim JI, Schuller-Lewis GB et al (2007) CpG oligodeoxynucleotide-enhanced humoral immune response and production of antibodies to prion protein PrPSc in mice immunized with 139A scrapie-associated fibrils. J Leukoc Biol 81(6):1374–1385
26. Jimenez-Huete A, Alfonso P, Soto C, Albar JP, Rabano A, Ghiso J, Frangione B (1998) Antibodies directed to the carboxyl terminus of amyloid beta-peptide recognize sequence epitopes and distinct immunoreactive deposits in Alzheimer's disease brain. Alzheimers Reports 1(1):41–47
27. Asuni AA, Pankiewicz JE, Sadowski MJ (2013) Differential molecular chaperone response associated with various mouse adapted scrapie strains. Neurosci Lett 538:26–31
28. Asuni AA, Guridi M, Pankiewicz JE, Sanchez S, Sadowski MJ (2014) Modulation of amyloid precursor protein expression reduces beta-amyloid deposition in a mouse model. Ann Neurol 75(5):684–699. https://doi.org/10.1002/ana.24149
29. Burgess A, Vigneron S, Brioudes E, Labbe JC, Lorca T, Castro A (2010) Loss of human Greatwall results in G2 arrest and multiple mitotic defects due to deregulation of the cyclin B-Cdc2/PP2A balance. Proc Natl Acad Sci U S A 107(28):12564–12569. https://doi.org/10.1073/pnas.0914191107
30. McCloy RA, Rogers S, Caldon CE, Lorca T, Castro A, Burgess A (2014) Partial inhibition of Cdk1 in G 2 phase overrides the SAC and decouples mitotic events. Cell Cycle 13(9):1400–1412. https://doi.org/10.4161/cc.28401
31. Wisniewski HM, Sadowski M, Jakubowska-Sadowska K, Tarnawski M, Wegiel J (1998) Diffuse, lake-like amyloid-beta deposits in the parvopyramidal layer of the presubiculum in Alzheimer disease. J Neuropath Exp Neurol 57(7):674–683
32. Adler J, Parmryd I (2010) Quantifying colocalization by correlation: the Pearson correlation coefficient is superior to the Mander's overlap coefficient. Cytometry 77((8):733–742. https://doi.org/10.1002/cyto.a.20896
33. Costes SV, Daelemans D, Cho EH, Dobbin Z, Pavlakis G, Lockett S (2004) Automatic and quantitative measurement of protein-protein colocalization in live cells. Biophys J 86(6):3993–4003. https://doi.org/10.1529/biophysj.103.038422
34. Utku Y, Dehan E, Ouerfelli O, Piano F, Zuckermann RN, Pagano M, Kirshenbaum K (2006) A peptidomimetic siRNA transfection reagent for highly effective gene silencing. Mol BioSyst 2(6–7):312–317
35. Tzaban S, Friedlander G, Schonberger O, Horonchik L, Yedidia Y, Shaked G, Gabizon R, Taraboulos A (2002) Protease-sensitive scrapie prion protein in aggregates of heterogeneous sizes. Biochemistry 41(42):12868–12875
36. Pastrana MA, Sajnani G, Onisko B, Castilla J, Morales R, Soto C, Requena JR (2006) Isolation and characterization of a proteinase K-sensitive PrPSc fraction. Biochemistry 45(51):15710–15717. https://doi.org/10.1021/bi0615442
37. Daude N, Lehmann S, Harris DA (1997) Identification of intermediate steps in the conversion of a mutant prion protein to a scrapie-like form in cultured cells. J Biol Chem 272(17):11604–11612
38. Lehmann S, Harris DA (1996) Mutant and infectious prion proteins display common biochemical properties in cultured cells. J Biol Chem 271(3):1633–1637
39. Liberski PP, Sikorska B, Hauw JJ, Kopp N, Streichenberger N, Giraud P, Boellaard J, Budka H et al (2010) Ultrastructural characteristics (or evaluation) of Creutzfeldt-Jakob disease and other human transmissible spongiform encephalopathies or prion diseases. Ultrastruct Pathol 34(6):351–361. https://doi.org/10.3109/01913123.2010.491175
40. Sikorska B, Liberski PP, Giraud P, Kopp N, Brown P (2004) Autophagy is a part of ultrastructural synaptic pathology in Creutzfeldt-Jakob disease: a brain biopsy study. Int J Biochem Cell Biol 36(12):2563–2573. https://doi.org/10.1016/j.biocel.2004.04.014
41. Feraudet C, Morel N, Simon S, Volland H, Frobert Y, Creminon C, Vilette D, Lehmann S et al (2005) Screening of 145 anti-PrP monoclonal antibodies for their capacity to inhibit PrPSc replication in infected cells. J Biol Chem 280(12):11247–11258
42. Scott MR, Groth D, Tatzelt J, Torchia M, Tremblay P, DeArmond SJ, Prusiner SB (1997) Propagation of prion strains through specific conformers of the prion protein. J Virol 71(12):9032–9044
43. Prusiner SB, Scott MR, DeArmond SJ, Cohen FE (1998) Prion protein biology. Cell 93:337–348
44. Sevigny J, Chiao P, Bussiere T, Weinreb PH, Williams L, Maier M, Dunstan R, Salloway S et al (2016) The antibody aducanumab reduces Abeta plaques in Alzheimer's disease. Nature 537(7618):50–56. https://doi.org/10.1038/nature19323
45. Novak P, Schmidt R, Kontsekova E, Zilka N, Kovacech B, Skrabana R, Vince-Kazmerova Z, Katina S et al (2017) Safety and immunogenicity of the tau vaccine AADvac1 in patients with Alzheimer's disease: a randomised, double-blind, placebo-controlled, phase 1 trial. The Lancet Neurol 16(2):123–134. https://doi.org/10.1016/S1474-4422(16)30331-3
46. West T, Hu Y, Verghese PB, Bateman RJ, Braunstein JB, Fogelman I, Budur K, Florian H et al (2017) Preclinical and clinical development of ABBV-8E12, a humanized anti-tau antibody, for treatment of Alzheimer's disease and other tauopathies. J Prev Alz Dis 4(4):236–241. https://doi.org/10.14283/jpad.2017.36
47. Masliah E, Rockenstein E, Adame A, Alford M, Crews L, Hashimoto M, Seubert P, Lee M et al (2005) Effects of alpha-synuclein immunization in a mouse model of Parkinson's disease. Neuron 46(6):857–868
48. Ward HJT, Head MW, Will RG, Ironside JW (2003) Variant Creutzfeldt-Jakob disease. Clin Lab Med 23(1):87–108
49. Peden AH, Head MW, Ritchie DL, Bell JE, Ironside JW (2004) Preclinical vCJD after blood transfusion in a PRNP codon 129 heterozygous patient. Lancet 364(9433):527–529
50. Peden A, McCardle L, Head MW, Love S, Ward HJ, Cousens SN, Keeling DM, Millar CM et al (2010) Variant CJD infection in the spleen of a neurologically asymptomatic UK adult patient with haemophilia. Haemophilia 16(2):296–304
51. Bishop MT, Diack AB, Ritchie DL, Ironside JW, Will RG, Manson JC (2013) Prion infectivity in the spleen of a PRNP heterozygous individual with subclinical variant Creutzfeldt-Jakob disease. Brain 136:1139–1145. https://doi.org/10.1093/brain/awt032
52. Bishop MT, Hart P, Aitchison L, Baybutt HN, Plinston C, Thomson V, Tuzi NL, Head MW et al (2006) Predicting susceptibility and incubation time of human-to-human transmission of vCJD. The Lancet Neurology 5(5):393–398. https://doi.org/10.1016/S1474-4422(06)70413-6
53. Mok T, Jaunmuktane Z, Joiner S, Campbell T, Morgan C, Wakerley B, Golestani F, Rudge P et al (2017) Variant Creutzfeldt-Jakob disease in a patient with heterozygosity at PRNP codon 129. N Engl J Med 376(3):292–294. https://doi.org/10.1056/NEJMc1610003
54. Collinge J, Whitfield J, McKintosh E, Beck J, Mead S, Thomas DJ, Alpers MP (2006) Kuru in the 21st century—an acquired human prion disease with very long incubation periods. Lancet 367(9528):2068–2074
55. Diack AB, Will RG, Manson JC (2017) Public health risks from subclinical variant CJD. PLoS Pathog 13(11):e1006642. https://doi.org/10.1371/journal.ppat.1006642
56. Urwin PJ, Mackenzie JM, Llewelyn CA, Will RG, Hewitt PE (2016) Creutzfeldt-Jakob disease and blood transfusion: updated results of the

UK Transfusion Medicine Epidemiology Review Study. Vox Sang 110(4):310–316. https://doi.org/10.1111/vox.12371

57. Gill ON, Spencer Y, Richard-Loendt A, Kelly C, Dabaghian R, Boyes L, Linehan J, Simmons M et al (2013) Prevalent abnormal prion protein in human appendixes after bovine spongiform encephalopathy epizootic: large scale survey. BMJ 347:f5675. https://doi.org/10.1136/bmj.f5675
58. Song CH, Furuoka H, Kim CL, Ogino M, Suzuki A, Hasebe R, Horiuchi M (2008) Effect of intraventricular infusion of anti-prion protein monoclonal antibodies on disease progression in prion-infected mice. J gen Virol 89:1533–1544. https://doi.org/10.1099/vir.0.83578-0
59. Luginbuhl B, Kanyo Z, Jones RM, Fletterick RJ, Prusiner SB, Cohen FE, Williamson RA, Burton DR et al (2006) Directed evolution of an anti-prion protein scFv fragment to an affinity of 1 pM and its structural interpretation. J Mol Biol 363(1):75–97. https://doi.org/10.1016/j.jmb.2006.07.027
60. Padiolleau-Lefevre S, Alexandrenne C, Dkhissi F, Clement G, Essono S, Blache C, Couraud JY, Wijkhuisen A et al (2007) Expression and detection strategies for an scFv fragment retaining the same high affinity than Fab and whole antibody: implications for therapeutic use in prion diseases. Mol Immunol 44(8):1888–1896. https://doi.org/10.1016/j.molimm.2006.09.035
61. Wuertzer CA, Sullivan MA, Qiu X, Federoff HJ (2008) CNS delivery of vectored prion-specific single-chain antibodies delays disease onset. Mol Ther 16(3):481–486. https://doi.org/10.1038/sj.mt.6300387
62. Moda F, Vimercati C, Campagnani I, Ruggerone M, Giaccone G, Morbin M, Zentilin L, Giacca M et al (2012) Brain delivery of AAV9 expressing an anti-PrP monovalent antibody delays prion disease in mice. Prion 6(4):383–390. https://doi.org/10.4161/pri.20197
63. Klohn PC, Farmer M, Linehan JM, O'Malley C, Fernandez de Marco M, Taylor W, Farrow M, Khalili-Shirazi A et al (2012) PrP antibodies do not trigger mouse hippocampal neuron apoptosis. Science 335(6064):52. https://doi.org/10.1126/science.1215579